Electrical Engineering (2023) 105:827–851
https://doi.org/10.1007/s00202-022-01700-7

ORIGINAL PAPER

SIPS-based resilience augmentation of power system network

Nilesh Kumar Rajalwal[1] · **Debomita Ghosh**[1]

Received: 8 December 2021 / Accepted: 27 November 2022 / Published online: 19 December 2022

Abstract
Natural calamities that include heavy storms, earthquakes, snowfall, and drought/heat waves are now predominant over the world. These natural calamities cause high impact low frequency (HILF) events, such as multi-location faults and multi-area stressed conditions, that may cause large blackouts and reduce system resilience. This paper proposes a system integrity protection scheme (SIPS) to accurately identify the multi-location faults and multi-area stressed system conditions. The proposed SIPS accurately detects the multi-location faults for synchronized operation of distance relay and simultaneously provides backup distance relay blocking in higher operating zones, during stressed system conditions. For the entire operation, data from WAMS are used to first detect the abnormal operating areas followed by identification of vulnerable buses in the system. Further, by comparing the phase angles of transmission lines connected to vulnerable buses, faulted lines are identified. The effectiveness of the method is tested for multiple scenarios carried out on the WSCC 9-bus system and New England 39-bus system in MATLAB/Simulink platform. For practical implementation, the performance is validated on a 4-bus test network on Typhoon hardware in loop (HIL) system. Adequate and synchronized relay operation results in the augmentation of resiliency in the power system network. Calculated resistance indices reflect increase in transmission capacity up to 140%, load loss reduction percent up to 0%, and improvement in the active power deficiency up to 57% during different operating conditions for considered test systems.

Keywords System integrity protection schemes (SIPS) · Multi-location fault · Power system resiliency · Distance relay · Phasor measurement unit (PMU) · High impact low frequency (HILF) events

Abbreviations

V_{ST}	Steady-state bus voltage matrix
I_{ST}	Steady-state branch current matrix
I_{ST}	Steady-state branch current matrix
V_M	Measured bus voltage matrix
I_M	Measured branch current matrix
Z_{AB}	Impedance of section AB
$\delta_{vi\_}$	Phase angle between voltage and current
P	Active power flow
Q	Reactive power flow
L_{ni}	Load demand under normal condition
L_{di}	Actual load demand during disaster
C_{k_d}	Power flowing in link k during disaster
G_{g_d}	Real power output of unit g during disaster
SIPS	System integrity protection scheme
HILF	High impact low frequency
WAMS	Wide-area monitoring system
PMU	Phasor measurement unit
ANN	Artificial neural network
NIAC	National infrastructure advisory council
CR	Current ratio
ACR	Area current ratio
ACR_{TH}	Threshold value of area current ratio
CLPP	Current load loss percent
ATCS	Available transfer capacity of section
APDA	Available power deficiency in area
AOA	Abnormal operating area

✉ Nilesh Kumar Rajalwal
nileshrajalwal@bitmesra.ac.in

Debomita Ghosh
debomita.ghosh@bitmesra.ac.in

[1] Department of EEE, Birla Institute of Technology Mesra, Ranchi, India

1 Introduction

Due to climate change, extreme natural events such as heavy storms, earthquakes, snowfall, and drought/heat waves, become more frequent in the past few years. These extreme events cause multiple-location faults system conditions that are responsible for cascaded system failure and wide-area blackout. Local measurement-based distance relays are very fast, especially in zone-I but suffers from asynchronous tripping at either end of the line during specific faulty conditions. Also, local protection schemes are not sufficient to protect the system during multiple-location faults. During the HILF events, the system also faces severely stressed conditions. Due to the large area on RX-diagram, the distance relay higher operating zones specially zone-III is severely affected by these stressed conditions. The impedance seen by local measurement-based distance relay during such conditions may come in the zone-III characteristic of the relay and increases the chances of relay mal-operation.

In the last few years, several cases are observed of distance relay mal-operation that initiates large area blackouts [1, 2]. Modern communication and protection technology has guided for development of a WAMS-based SIPS for a large power system network. PMUs, the fundamental component of WAMS, are used for measuring the time-synchronized phasor data of a power system network. The PMU data have a high sampling rate and are time-tagged by a global positioning system (GPS), which substantially enhances the power system monitoring and control over the conventional protection system. PMU-assisted SIPS utilizes the data from WAMS to take the control actions such as load shedding, generation rejection, and relay tripping/blocking for safe and reliable operation of the power system. SIPS is the wide-area protection schemes that are planned to detect abnormal operating conditions and initiate pre-planned automatic corrective actions based on system studies. SIPS utilizes local as well as global data to detect abnormal system conditions and to decide on the course of action and take appropriate corrective measures [3].

1.1 Literature review

The dependency of modern society on electrical power is very high. For the availability of electric power at our end, the grid must ensure the transmission of power from generating stations to load centers through an interconnected transmission network. In the past few years, this interconnected power network collapsed due to various HILF events. The Hud-hud cyclone in AP, India [4], and Hurricane Sandy in USA [5] severely affected the power system as well as the large population. Peak summer affected the hydel power generation and the increased load demand caused Indian grid blackout and a high cost of power purchase in Rajasthan, India [6, 7]. Earthquake in Bhuj, India, and ice-storm in the USA and Canada also affected the electricity supply of millions of people [7, 8]. These events lead to the tripping of multiple transmission lines and multi-location fault scenarios.

From the past HILF events, it is clear that multi-location faults and multi-area stressed conditions are common during these events. These multi-location faults and multi-area stressed conditions are responsible for the mal-operation of distance relays. Few authors reported fault identification strategies for multi-location faults. A multi-fault location strategy based on a fault fitting factor is proposed in [9]. A correlation matrix is formed by the fault equivalent model and node voltage equations of the faulted branch. Then, the virtual fault location and the fitting degree of each fault combination are calculated. In [10], a fault diagnosis framework is proposed that identifies the nodes of multiple faults. The probabilistic neural network is trained using the eigenvalues of system voltage. The final diagnosis is done by an adaptive neuro-fuzzy inference system. In [11], discrete wavelet transform-based artificial neural network (DWT-ANN) modules are used to identify the multi-location fault using voltage and current signals in less than 10 ms. This method also avoided any mal-operation of other healthy transmission lines. Another fault location estimation scheme using ANN is proposed for multi-location faults and transforming faults occurring in thyristor-controlled series compensated lines in [12]. DB-4 wavelets are utilized for the processing of current and voltage signals. This algorithm identified the fault location with an accuracy of 99–99.999%. In [13], a multi-location fault is interpreted by utilizing Smoothed Pseudo Wigner-Ville distribution and Hilbert transform. Finally, the proposed indices are calculated to identify the multi-location fault.

The methods proposed in [9–13] are effective to find the multi-location faults. However, methods [10–12] are based on training the data sets, and as the system complexity increases, the requirement for training sets increases. Also, with the addition of new components in the network, the algorithms require new training. None of the methods [9–13] provides the synchronous tripping of the relay at either end of transmission lines, also none of these methods apply the SIPS technology to find the multi-location fault. Only method proposed in [13] is validated on a real-time simulator platform for identification of multi-location faults. Also, no method provides the detail about the backup protection of distance relay in higher operating zones. Table 1 represents the comparison of existing literature on the multi-location fault assessment.

The distance relay mal-operation in higher operating zones is one of the subsequent effects of multi-area stressed system conditions. A survey is presented in [14] to explain the reason and consequences due to the mal-operation of distance

Table 1 Comparison of existing literature on multilocation fault assessment

Ref	Problem	Method	Solution	Feature	Limitations			
					Training requirements after network changes	Protection in higher operating zones	Implemented on RTDS	Synchronized tripping
[9]	Multi-location fault	Forming nodal admittance matrix and correlation coefficient	Development of fault equivalent model	Low computational burden	No	No	No	No
[10]	Multiple fault diagnosis	PNN + ANFIS	Use of eigenvalues of the correlation matrix	Two-phase classification approach	Yes	No	No	No
[11]	Multi-location fault	DWT + ANN	One DWT + ANN module for fault detection and second for classification	The algorithm detects/classifies fault in less than 10 ms	Yes	No	Yes	No
[12]	Multi-location fault	DWT + ANN		Detection of fault in TCSC compensated lines	Yes	No	No	No
[13]	Multi-location fault	SPWVD and Hilbert transform	Time–frequency analysis	Detecting fault within 0.01 s	No	No	Yes	No

relay. The survey suggests that remote measurements along with a communication-assisted protection scheme prevent the distance protection mal-operation. Few authors reported the application of SIPS for adequate operation of distance relay [15–19]. Distance relay mal-operation under stressed system conditions is blocked by developing a SIPS that utilizes an index based on angle derived from PMUs and rate of change of active power [15]. A deterministic-probabilistic approach is proposed in [16] to identify the critical lines that may be responsible for cascaded system outage after zone-III operation of distance relay. For blocking the mal-operation of distance relay, this approach identified the critical lines that have the highest contribution to cascading failure. A fast fault detection method based on support vector machine (SVM) under impedance fault detector is proposed in [17]. Further probabilistic neural network and S-transform are utilized to discriminate the faulty condition from the stressed system condition. SIPS for enhancing the situational awareness (SA) of the power system is proposed in [18]. This method utilizes PMU to detect the sensitive region within a network. Also, estimated peak time and settling time of voltage phasors are utilized to differentiate between single location fault and stressed system conditions. In [19], the faulty lines are identified by utilizing a new voltage-based index derived from dynamic state estimation. For dynamic state estimation, Cubature Kalman filtering is utilized for full system observability and to take appropriate actions for backup zones.

It is observed that most of the methods suggested in [15–19] although use SIPS but are effective for adequate operation of higher operating zones of distance relay for single location fault and stressed conditions. The coordinated operation of distance relay higher operating zones using SIPS during multi-location faults and multi-area stressed

condition is a significant field of research. There are substantial chances of mal-operation of distance relay in higher operating zones during stressed system conditions. This mal-operation reduces the resilience of the system.

The term 'resilience' consists of several elements ranging from resisting a disruptive event to recovering from that event. As no standard indices are available for resilience, estimation of resiliency after implementing a protection scheme is a difficult task. However, various methods are proposed for the resilience assessment of power system. The resiliency assessment methods are broadly classified as qualitative and quantitative assessments [20]. Various quantitative assessment approaches are proposed by different authors [21–24]. In [21], multiple indices are proposed to measure the effect of hazards on the power system. Outage index, resistance, and restoration speed are utilized to quantify resiliency. This framework may further be used to enhance the planning design and operation of the power system under hazardous conditions. Another resiliency index is proposed in [22][2 based on six different factors, i.e., critical fraction, network topology, graph diameter, average path length, betweenness centrality, algebraic connectivity, and clustering coefficient. The quantification of resiliency using different network topology parameters is proposed in [23]. This method stressed a minimal number of switching to restore the critical loads. In [24], time-dependent resiliency metrics are proposed that include four different matrices that are the rate of degradation, level of degradation, the extensiveness of degradation, and rate of recovery to discriminate operational and infrastructure resiliency.

The qualitative assessment techniques as in [25–31] discovered the weak zones in a power network to enhance resiliency. For resiliency assessment, the three components of resilience are classified as robustness, resourcefulness, and recovery [25]. These components are further divided up to level five and then related indices are computed for resiliency assessment. In [26], a similar method is adopted in which the indices are first classified as preparedness, mitigation measures, response capabilities, and recovery. These are further classified up to level six. Qualitative assessment based on power metrics related to load mismatch, supplied and unsupplied load, and available generation capacity are proposed in [27, 28]. Duration metric that is based on load curtailment, customer outage duration, and average interruption duration is proposed in [29]. Frequency metrics are based on loss of load frequency, and frequency of customer disconnections is proposed in [30, 31]. Various resiliency indices are discussed for the resiliency assessment in [25–31] but none of these indices are utilized to represent the resiliency augmentation of the power system network with the incorporation of SIPS.

1.2 Major contribution

The major contributions are as follows:

- Proposed a SIPS for accurate identification of multi-location faults and synchronized tripping of distance relay at either end of lines.
- During extreme events, the system network is severely stressed. The proposed SIPS effectively discriminates between a faulty and stressed area.
- Schemed SIPS assists in the blocking of higher operating zones of distance relay during severely stressed conditions.
- Resilience augmentation due to blocking of distance relay mal-operation in higher operating zones during stressed conditions and synchronized tripping during multi-location faults.
- Estimation of resistance indices to represent the resiliency accession in different network scenarios using the proposed method.
- Validation of proposed SIPS using the data obtained from real-time simulator (Typhoon HIL).
- Comparison of the proposed method with conventional digital distance protection and existing literature is done to prove the efficacy of the proposed method.

The remaining paper is organized as follows: In Sect. 2, effect of HILF events on distance relay performance is briefed. Section 3 outlines the proposed SIPS strategy. Section 4 presents the resiliency assessment indices for the schemed SIPS. Section 5 analyzes the effectiveness of the proposed methodology to protect the system during extreme events through simulation and HIL implementation. Section 6 concludes the work.

2 Effect of HILF events on Distance Relay performance

Distance relays are extremely prevalent for primary and backup protection of long transmission lines. The relays operate when the impedance of the line falls inside its characteristic area. A distance relay R_1 as shown in Fig. 1 at bus-*B* typically has three-zone characteristics. The zone-I boundary for distance relay is 80% of line length. The zone-II boundary covers the complete line along with a half-length of the immediate shortest line. Similarly, zone-III covers the total length and 110% of the immediate longest line. Distance relay calculates the apparent impedance at relay location that is further dependent on the line power flow and calculated using Eq. (1) [32].

$$Z_{\mathrm{BC}} = \left[\frac{P_{\mathrm{BC}}}{P_{\mathrm{BC}} + Q_{\mathrm{BC}}} + j\frac{Q_{\mathrm{BC}}}{P_{\mathrm{BC}} + Q_{\mathrm{BC}}}\right]|V_B|^2 \tag{1}$$

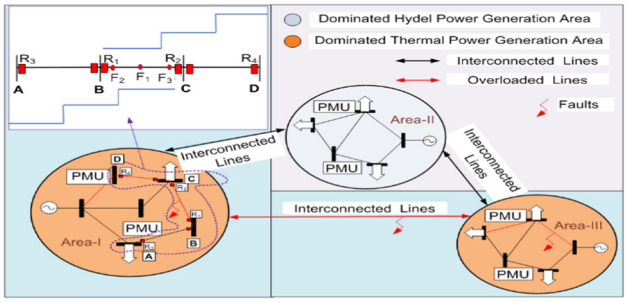

Fig. 1 Multi-area network to representing multi-location fault events and its effect on distance relay operation

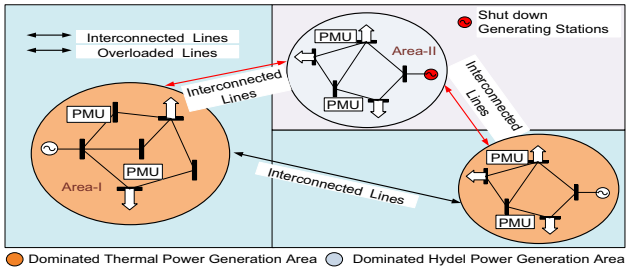

Fig. 2 Multi-area network representing Multi-area stressed condition and its effect on distance relay operation

Here, P and Q are the active and reactive power flow between bus-B and bus-C, and V_B is the voltage of bus-B, respectively.

The conventional distance protection is prone to asynchronous tripping at either end of line. In Fig. 1, both relays R_1 and R_2 provide instantaneous tripping for fault F_1. However, fault F_2 is in zone-I of relay R_1 and in zone-II of relay R_2. In this scenario, R_1 provides instantaneous tripping while R_2 a delayed tripping. This asynchronous tripping may lead the system toward a cascaded blackout.

Figure 1 also presents multi-location faults, i.e., fault in Area-I and Area-III that are hit by the same extreme weather conditions. Due to these multi-location faults, the power swing phenomenon persists in the transmission network. Distance relays are very prone to operate during these power swings and may mal-operate in such conditions. The mal-operation of distance relay may lead to cascaded system failure.

During multi-area stressed system conditions, the chances of load encroachment and voltage instability are very high. During load encroachment, the impedance measured by distance relay is determined by the loadability limit, as the specific power factor exceeds [33]. Increased load in the selective area of the power system reduces the impedance seen by the relay. During extreme events, the network may also face a shortage of reactive power due to line limits, increase in load reactive power consumption, or failure of generating plants. A reduction in reactive power causes a reduction in the voltage of the system, which further reduces the impedance seen by the relay. The zone-III characteristic of distance relay has a large area, and reduced impedance seen by a relay may come under the zone-III characteristic and causes mal-operation.

A multi-area stressed condition is represented by a three-area network in Fig. 2. In this network, the major power generation in Area-I and Area-III is by thermal power stations. Area-II has dominating hydel power generation. In a draught condition, the power generation capacity of Area-II decreases. The peak summer increases the load in all the areas causing overloading of interconnected transmission lines leading to multi-area stressed conditions.

Advancements in microprocessor and communication technologies enabled a new dimension to the protection schemes. These advancements in technologies facilitate the SIPS to preserve the power system integrity under all operating conditions.

3 Schemed SIPS Strategy

Protection algorithm under extreme natural events has two major tasks: Firstly, identification and isolation of faulty portions and secondly to block the operation of relays that are under stressed conditions but are in the no-fault region. For this purpose, SIPS strategy is significant and discussed in this section that enables synchronized relay tripping, finds the multi-location faults, discriminates the faults with multi-area stressed conditions and operates utilizing local or global information for needful action. The flowchart of the proposed algorithm is shown in Fig. 3. The conventional protection scheme is modified to facilitate synchronized tripping for fault locations F_2 and F_3 shown in Fig. 4a, and thus enhance the protection scheme. For fault location F_1, the local SIPS initiates the tripping command instantaneously for either end of the line. However, for a fault at location F_2 in Fig. 4a, the impedance seen by relay R_1 will come under the zone-I setting of relay R_1, i.e., $Z_{\text{set\_I\_R1}}$ and the impedance seen by relay R_2 will come under the zone-II setting of relay R_2, i.e., $Z_{\text{set-II\_R2}}$. Similarly, for a fault at location F_3 in Fig. 4a, the impedance seen by relay R_2 will come under the zone-I setting of relay R_2, i.e., $Z_{\text{set\_I\_R2}}$ and the impedance seen by relay R_1 will come under the zone-II setting of relay R_1, i.e., $Z_{\text{set\_II\_R1}}$. The proposed algorithm in these cases actuate relays at either end of the line using global SIPS and initiates synchronous tripping.

The proposed SIPS assists the distance relay performance in the higher operating zones during stressed system conditions. If stressed network conditions take the impedance of relay R_3 or R_4 under zone-III of their relay setting, i.e., $Z_{\text{set\_III\_R3}}$ and $Z_{\text{set\_III\_R4}}$, respectively, the proposed SIPS will

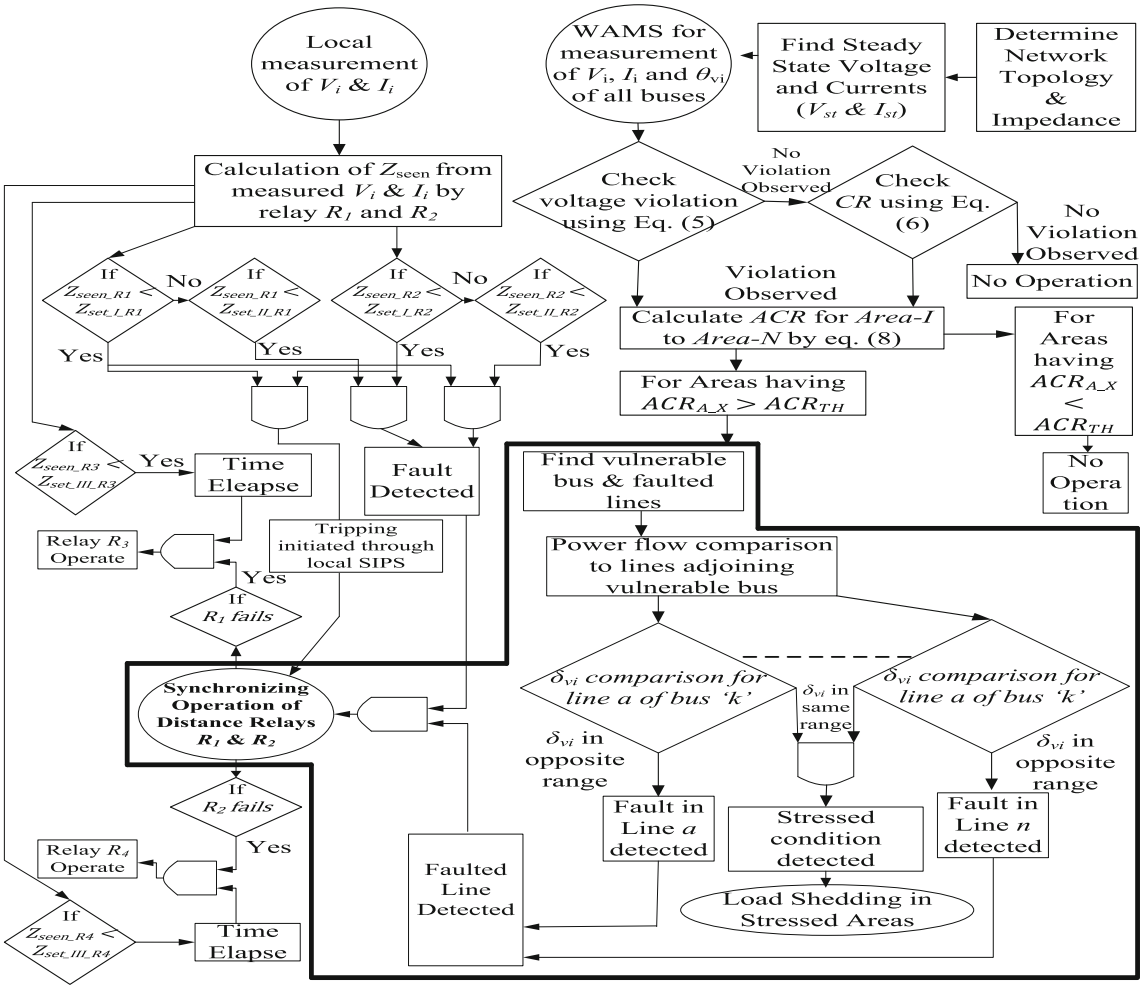

Fig. 3 Flowchart of the proposed System Integrity Protection Scheme

not initiate the operation of either relay. The algorithm will first detect the abnormality in the system and if no fault condition is detected, it will block the unnecessary tripping of distance relay in higher operating zones. Also, in case of failure in the primary protection, i.e., by relay R_1 or R_2, the backup protection is provided by relay R_3 and R_4 in collaboration with the proposed SIPS.

The execution sequence of the proposed SIPS is illustrated as follows:

(a) Determination of steady-state voltage and current values:

The steady-state voltages and currents are determined with the help of network data and topology. The steady-state voltage and currents matrix for a network having n buses and m lines is represented in Eq. (2).

$$V_{ST} = \left[V_{1\_ST}\, V_{2\_ST}\, V_{3\_ST} \ldots\ldots\ldots V_{n\_ST}\right] \;\&\; I_{ST} = \left[I_{1\_ST}\, I_{2\_ST}\, I_{3\_ST} \ldots\ldots\ldots I_{m\_ST}\right] \tag{2}$$

If the system has P number of areas with three transmission lines in each area, the steady-state line current matrix for each area is represented in Eq. (3).

$$I_{A\_P\_ST} = \left[\, I_{a\_ST}\; I_{b\_ST}\; I_{c\_ST} \,\right] \tag{3}$$

where $I_{A\_P\_ST}$ is the steady-state line current matrix for Area-P under rated conditions and I_{a_ST}, I_{b_ST} and I_{c_ST} are the line currents of lines a, b and c, respectively, in Area-P.

(b) Determination of voltage and current violations:

In real-time conditions, PMUs are utilized to measure the voltage and current phasors of the complete transmission network. PMU is a device that acquires three-phase voltages and currents from potential transformers and current transformers, samples them using a common synchronizing clock signal obtained from GPS, and then computes discrete Fourier transforms (DFT) on the resulting current and voltage phasors (magnitude with phase angle). In practice, most

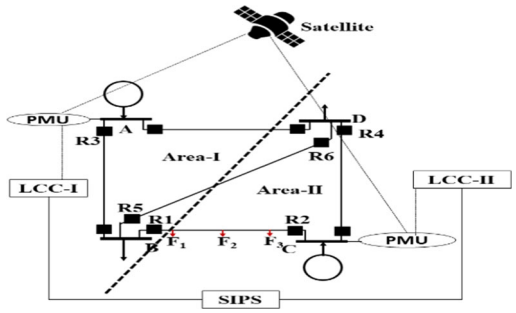

(a) 4-Bus System with Fault in Section *BC*

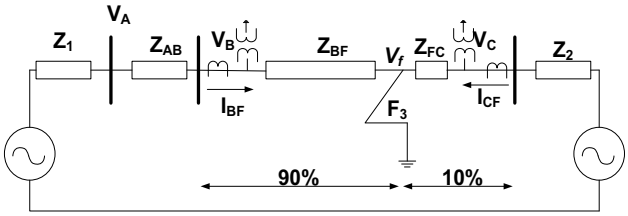

(b) Eq. Circuit of fig. 4(a) for fault F_3

Fig. 4 4-Bus System during the faulted condition

PMUs utilize DFT for the identification of the magnitude and phase of the desired signal [34]. Thus, the magnitude and phase of the fundamental component of measured voltage and the current signal are obtained from DFT for processing the algorithm.

With modern technology, the latency of PMU and PDC systems is reduced drastically. *P* class PMUs having low latency are placed at optimum locations within networks. PMUs measurements are collected at a reporting rate of 25–50 samples per second. The collected samples are time synchronized thus at a central location; a comprehensive view of the whole grid is available all-in real-time. The collected data are communicated to PDC through fiber optics at a very high speed and the reporting rates are 60 frames/s [15]. Received data in PDC are aggregated and relayed using a two-way communication system to local control centers (LCCs), which co-ordinate their actions interacting with a SIPS.

The measured voltage and currents matrix is represented in Eq. (4).

$$\begin{aligned} V_M &= \left[V_{1\_M}\, V_{2\_M}\, V_{3\_M} \ldots\ldots\ldots V_{n\_M}\right] \& \\ I_M &= \left[I_{1\_M}\, I_{2\_M}\, I_{3\_M} \ldots\ldots\ldots I_{m\_M}\right] \end{aligned} \tag{4}$$

The proposed algorithm compares the voltage and current violations at each bus and transmission line continuously to find the abnormal condition in the power system. The voltage deviation is expressed in Eq. (5)

$$\Delta V = \frac{V_{i\_M} - V_{i\_ST}}{V_{i\_ST}} * 100\% \tag{5}$$

The voltage violations are observed if $|\Delta V| > 5\%$ [13].

In the power system, additional types of equipment such as FACTS devices, tap changing transformers, and capacitor banks are utilized to maintain the voltage level during stressed conditions. Thus, considering only voltage violation as an indicator for the normal/ abnormal state of the system is not a decent alternative. Hence, the current ratio (CR) is calculated to confirm the violation in the system. The CR in each transmission line is defined in Eq. (6).

$$\mathrm{CR} = \frac{I_{i\_j\_M}}{I_{i\_j\_\mathrm{ST}}} \tag{6}$$

The system will be in an abnormal operating state, if |CR|> 1.5 [18]. If violations are observed utilizing Eqs. (5) and (6), the system condition is considered to be an abnormal state. After the abnormality detection, the abnormal operating areas are detected.

(c) Determination of the abnormal areas and vulnerable buses using PMUs Data:

The algorithm proposed in [18] is modified to find the multi-location fault or multi-area stressed system condition. The measured line current matrix for Area-*P* is shown in Eq. (7)

$$I_{A\_P\_M} = \left[\, I_{a\_M}\ I_{b\_M}\ I_{c\_M} \,\right] \tag{7}$$

where $I_{A\_P\_M}$ is the measured line current matrix for Area-*P* and I_{a_M}, I_{b_M} and I_{c_M} are the measured line currents of lines *a, b* and *c*, respectively, in Area-*P*.

The area current ratio (ACR) for each area is calculated by taking the ratio of the maximum measured line current from the line current matrix of an area to the maximum steady-state line current from the steady-state line current matrix. The ACR for Area-*P* is shown in Eq. (8).

$$\mathrm{ACR}_{A\_P} = \frac{\max\left(I_{A\_P\_M}\right)}{\max\left(I_{A\_P\_\mathrm{ST}}\right)} \tag{8}$$

A particular area is detected in an abnormal operating condition if the ACR of that area is higher than the threshold value *ACR* ($\mathrm{ACR_{TH}}$). The value of $\mathrm{ACR_{TH}}$ is determined by simulating various faults at different locations and overloading conditions on the transmission network. In other words, an abnormal condition in Area-*P* is detected by Eq. (9)

$$\mathrm{ACR}_{A\_X} > \mathrm{ACR_{TH}} \tag{9}$$

If the condition mentioned in (9) is satisfied for any area, that area is categorized as an abnormal area, and the bus with maximum fault current in that area is treated as the vulnerable bus.

(d) Identification of fault for synchronized tripping:

The identified vulnerable buses are utilized to find the faulted line. The power flow direction at both ends of the lines connected to vulnerable buses is compared to find the faulted line.

This power flow direction is detected using the voltage and current phase angle. Optimally placed PMUs provide the real-time voltage and current phasors at each terminal of a network. The local control center (LCC) will get the control signal for synchronized tripping or blocking the relays based on the proposed SIPS. For understanding the above principle, a 4-bus system is shown in Fig. 4a is utilized.

The fault F_3 shown in Fig. 4a in section BC is assumed at 10% of line length from bus C. The zone-I protection of relay R_2 will operate for such faults. However, the relay R_1 at bus B will treat this fault in zone-II and thus initiates delayed tripping. The asynchronous tripping of relay R_1 and R_2 increases the chances of unwanted tripping of adjacent lines.

The equivalent circuit of a 4-bus system for a three-phase fault in section BC is shown in Fig. 4b, where V_A, V_B, and V_C are the voltage of buses A, B, and C, respectively. I_{BF} and I_{CF} are the fault currents from bus B and bus C, respectively. Z_{BF} and Z_{CF} are the impedance of the line to the fault point from terminals B and C. V_f is the voltage at the fault point and Z_f is the fault impedance. The current I_{BF} in section BC from terminal B is as in Eq. (10)

$$I_{\mathrm{BF}} = \frac{V_B - V_F}{Z_{\mathrm{BF}} + Z_F} \tag{10}$$

If the phase angle difference between the voltage V_B and current I_{BF} is represented by δ_{vi_B}, it can be computed by Eq. (11).

$$\delta_{vi\_B} = \arg\left(\frac{I_{BF}}{V_B}\right) \tag{11}$$

On placing the value of I_{BF} from Eqs. (10) to (11), Eq. (12) is achieved.

$$\delta_{vi\_B} = \arg\left(\frac{V_B - V_F}{(Z_{BF} + Z_F) * V_B}\right) \tag{12}$$

Taking V_B as a reference phasor, the impedance of the line is considered to be mostly inductive and Z_F to be resistive in nature in Eq. (12) makes the $arg(Z_{BF} + Z_F)$ in the range of (0°–90°). The value of $arg(V_B - V_F)$ lies between (−90° to 90°), thus, making the angle δ_{vi_B} in the range of (180°–360°).

Similarly, I_{CF} in section BC from terminal C is as in Eq. (13)

$$I_{CF} = \frac{V_C - V_F}{Z_{CF} + Z_F} \tag{13}$$

If the phase angle between the V_C and I_{CF} is represented by δ_{vi_C}, it is computed by Eq. (14).

$$\delta_{vi\_C} = \arg\left(\frac{I_{CF}}{V_C}\right) \tag{14}$$

On placing the value of I_{CF} from Eq. (13) to (14), Eq. (15) is attained.

$$\delta_{vi\_C} = \arg\left(\frac{V_C - V_F}{(Z_{CF} + Z_F) * V_C}\right) \tag{15}$$

As V_B is assumed as a reference phasor, the phase angle of V_B and V_C lies in the range of (0^0 to 90^0). In Eq. (15), the $arg((Z_{CF} + Z_F) * V_C)$ is in the range of (0°–180°). The value of $arg(V_C - V_F)$ lies between (−90° to 90°). It makes the angle δ_{vi_C} in the range of (0°–90°).

The angular difference between terminal B and C from Eq. (12) and (15) will be in the opposite range for the fault between terminals.

(e) Blocking of the distance relay in higher operating zone during multi-area stressed conditions:

Zone-III of distance relay is highly sensitive due to stressed system conditions and may cause mal-operation of distance relay in zone-III without any fault.

For the fault shown in Fig. 4a, R3 will provide backup protection in higher operating zone. This relay R_3 may also see impedance trajectory in zone-III due to stressed system condition and without any fault may mal-operate.

The angular difference as mentioned during the faulty condition in Eqs. (12) and (15) will not be present during stressed conditions. This is utilized to block the backup relay mal-operation in a higher operating zone.

The equivalent circuit of Fig. 4a with stressed condition is represented in Fig. 5, and the current in section BC during the stressed condition is represented by Eq. (16).

$$I_B = I_C = \frac{V_B - V_C}{Z_{BC}} \tag{16}$$

The phase angle difference between the voltage V_B and current I_B and voltage V_C and current I_C is as in Eq. (17)

$$\delta_{vi\_B} = \arg\left(\frac{I_B}{V_B}\right) \;\&\; \delta_{vi\_C} = \arg\left(\frac{I_C}{V_C}\right) \tag{17}$$

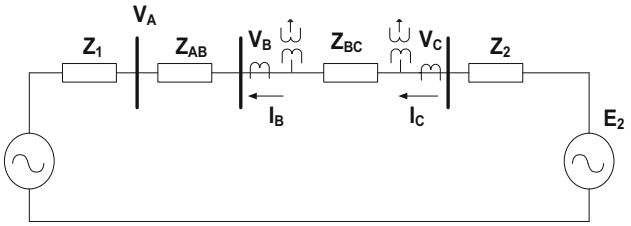

Fig. 5 Equivalent circuit of 4-bus system for stressed condition

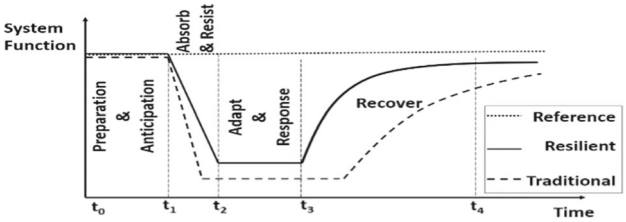

Fig. 6 Illustrative representation of resilience response of power system

On placing the values of I_B and I_C from Eq. (16) to (17), Eq. (18) is attained

$$\delta_{vi_B} = \arg\left(\frac{V_B - V_C}{Z_{BC} * V_B}\right) \;\&\; \delta_{vi_C} = \arg\left(\frac{V_B - V_C}{Z_{BC} * V_C}\right) \quad (18)$$

In Eq. (18), the angle δ_{vi_B} and δ_{vi_C} and both will be in the same range of (0°–90°) for no-fault conditions.

As no fault condition is detected by the proposed SIPS, no signal is fed to backup relay R_3, and is blocked mal-operation of the relay during the stressed condition.

Adequate operation of distance relays also enhances the resilience augmentation in the network. Thus, the resilience assessment is also done to achieve resiliency augmentation.

4 Resilience assessment indices for the proposed SIPS strategy

Resilience is progressively identified as a new parameter for designing the infrastructure and control strategies of a modern power system. A highly resilient system should be capable enough for fast restoration after any HILF event. An illustrative process of a resilient power system is presented in Fig. 6. In the preparation and anticipation phase (from t_0 to t_1), weather forecasting technologies are used to prepare the system for extreme events. At t_1, the disruption takes place, and the system resists the disruption and absorbs the changes by generation and load dispatching (from t_1 to t_2). From t_2 to t_3, system response such as islanding and switching of local generation takes place. After t_3, the system recovery is done by the maintenance of faulted lines, replacement of damaged equipment, switching on loads, and generation [35]. The power system is said to be resilient if the area covered under the resilience curve decreases. Practically, all these stages are different and separate methods are adopted to enhance the resilience in each of these processes. In the proposed work, the system response and robustness are improved by utilizing SIPS during a disaster-hit state. Proposed SIPS reduces the unwanted tripping of transmission lines that reduces the magnitude and the slope of resilience system function between t_1 to t_2. This reduces the area under the resilience curve and represents the resilience augmentation.

To assess resilience during a disaster-hit state, the during-disaster system resistance proposed in [36] is utilized. For each faulted scenario, three parameters, i.e., current load loss percent (CLLP), available transmission capacity of the section (ATCS), and active power deficiency in the area (APDA) are used to find the during-disaster system resistance.

CLLP shows the loss of load in the power system under natural events. It is represented by Eq. (19).

$$\text{CLPP} = \frac{\sum_{i=1}^{n}\left(L_{nl,i} - L_{dl,b}\right)}{\sum_{i=1}^{n} L_{nl,b}} \quad (19)$$

where $L_{nl,i}$ is the load demand of bus i under normal conditions; $L_{dl,b}$ is the actual load amount of bus b during disasters and n is the number of buses in the power system.

The ATCS represents the damage situation of the transmission section, and it is expressed as in Eq. (20).

$$\text{ATCS} = \sum_{j \in l_{\text{during}}} \left(C_{k,\max} - \left|C_{k,d}\right|\right) \quad (20)$$

Here, $C_{k,\max}$ is the upper limit of line k, $C_{k,d}$ is the power flowing in line k during disasters and l_{during} is the set of normal lines during disasters.

The APDA indicates the real power deficiency of the area where sufficient generation is not available. It is represented by Eq. (21)

$$\text{ADPI} = \sum_{i \in B_{\text{all}}} l_{i,\text{real},d} - \sum_{g \in G_{\text{during}}} G_{g,d} \quad (21)$$

where $l_{i,\text{real},d}$ is real power load demand of bus i, G_{during} is the normal operating units of the disaster area and $G_{g,d}$ is the during disasters real power output of unit g.

An improvement in these resistance indices represents the resilience augmentation during a disaster-hit state. Proposed SIPS improves these resistance indices and thus supports resilience augmentation.

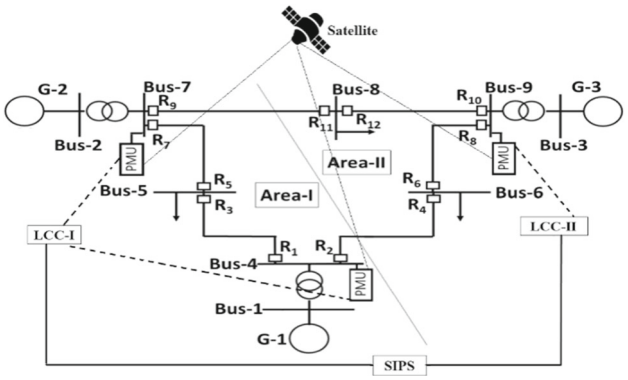

Fig. 7 WSCC 9-bus Test System [37]

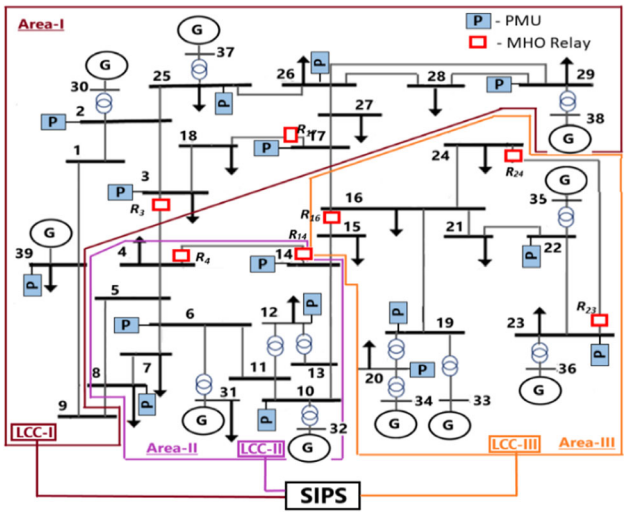

Fig. 8 New England 39-Bus Test system [7]

5 Simulation and HIL Implementation

In this section, the performance of the proposed algorithm represented in Fig. 5 is tested through multiple scenarios on WSCC 9-bus system and New England 39-bus system on MATLAB/ Simulink platform and proposed SIPS strategy is validated with a 4-bus test system in Typhoon HIL.

5.1 Steady-state performance of WSCC-9 bus and New England 39-bus system

A single line diagram of WSCC 9-bus test system is shown in Fig. 7. The system consists of six transmission lines, three generators at buses 1, 2, and 3, and three loads at buses 5, 6, and 8, respectively. Two different areas are considered in the system to test the performance of the proposed method.

The steady-state voltage and currents matrices are obtained with reference to Eq. (2) for WSCC 9-bus system as

$$V_{ST} = \left[V_{1_{ST}} V_{2_{ST}} V_{3_{ST}} \ldots\ldots\ldots V_{9ST}\right] \&$$
$$I_{ST} = \left[I_{7\_8\_ST} I_{5\_7\_ST} I_{4\_5\_ST} I_{4\_6\_ST} I_{6\_9\_ST} I_{8\_9\_ST}\right]$$

The steady-state line current matrices as represented using Eq. (3) for each area is represented as

$$I_{A\_1\_ST} = \left[\, I_{7\_8\_ST}\ I_{5\_7\_ST}\ I_{4\_5\_ST} \,\right]$$

$$I_{A\_2\_ST} = \left[\, I_{4\_6\_ST}\ I_{6\_9\_ST}\ I_{8\_9\_ST} \,\right]$$

where $I_{A\_1\_ST}$ and $I_{A\_2\_ST}$ are the steady-state line current matrix for Area-1 and Area-2, respectively, under rated conditions.

The steady-state bus voltage and line current phasors of WSCC 9-bus system are represented in Table 2.

The New England 39-bus test system shown in Fig. 8 consists of 10 generators. Optimally placed PMUs are represented in Fig. 8 which are utilized for real-time phasor measurements. Three different areas are considered in the system to test the performance of the proposed method. Each transmission line is associated with distance relays at both terminals, but in this analysis, only five relays are represented, i.e., R_3, R_4, R_{16}, R_{17}, and R_{23} which are utilized. The steady-state bus voltage and line current phasors of New England 39-bus system are as in Table 3.

5.2 Distance relay operation with proposed SIPS

Various scenarios are simulated on the considered test systems and discussed in this sub-section to find the effectiveness of the proposed algorithm. The performance is tested for the following scenarios:

(a) Distance relay performance with proposed SIPS during single location fault with the stressed condition.
(b) Distance relay performance with proposed SIPS during Fault at multiple locations.
(c) Distance relay performance in higher operating zones with proposed SIPS during stressed conditions.

(a) Distance relay performance with proposed SIPS during single location fault with the stressed condition

A LLL fault is applied at 10% of line length from bus 4 of L_{4_5} in Area-I for WSCC 9-bus system, as in Fig. 7 at 1.5 s. Additionally, a stressed system condition is created by increasing the load at bus 6 and bus 8 to 1.5 times their rated value, followed by switching off the alternator at bus-3.

During this faulty condition, the conventional protection scheme initiates asynchronous tripping. Figure 9 shows conventional three-zone characteristic with impedance locus of both relays R1 and R3, respectively, for protecting the line L_{4_5}. MHO relay R_1 detects the fault under zone-I and R_3

Table 2 V_{i_ST} and $I_{i\_j\_ST}$ of WSCC 9-bus system

Area	Bus (i)	V_{i_ST} (P.U.)	Line (i–j)	$I_{i\_j\_ST}$ (PU)
Area-I	2	1.025	L_{7-8}	0.2647
	5	0.9724	L_{5-7}	0.3188
	7	1.004	L_{4-5}	0.397
	1	1.04		
	4	0.9966		
Area-II	3	1.025	L_{4-6}	0.2155
	6	0.987	L_{6-9}	0.2844
	8	0.994	L_{8-9}	0.2945
	9	1.004		

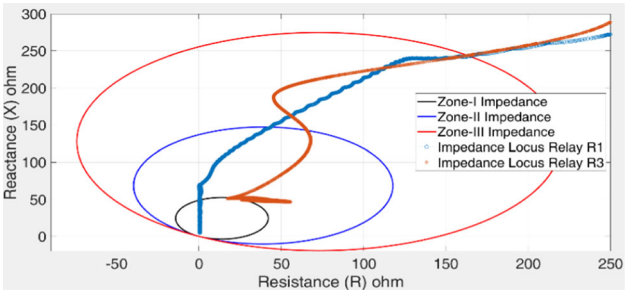

Fig. 9 MHO Relay R_1 and R_3 characteristic for fault in L_{4-5} and stressed system condition in WSCC 9-bus system

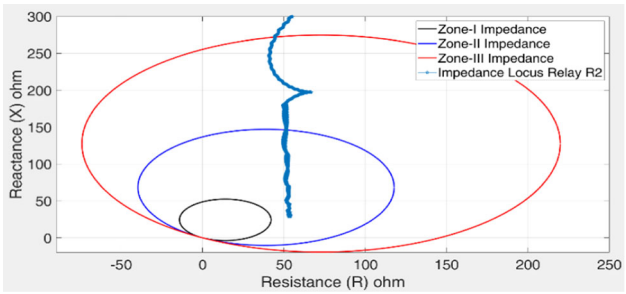

Fig. 10 MHO Relay R_2characteristic for fault in L_{4-5} and stressed system condition in WSCC 9-bus system

detects the fault under zone-II. As the faults are detected by either end of relays R_1 and R_3 in two different zones, it initiates the asynchronous tripping of relays and may start cascaded tripping. The conventional protection scheme also initiates mal-operation of relay in healthy section due to stressed system condition along with a fault. Relay R_2 at bus 4 sees a reduction in impedance, which comes under zone-II as shown in Fig. 10. The proposed SIPS enables the synchronous operation of relays R_1 and R_3 at either end of line and blocks the undesirable operation of relay R_2.

In the proposed SIPS, the real-time voltage and current phasors measured from PMU as referred in Eq. (4) is represented for WSCC 9-bus system.

$$V_M = \left[V_{1\_M}\, V_{2\_M}\, V_{3\_M} \ldots\ldots\ldots V_{9\_M}\right] \&$$

$$I_M = \left[I_{7\_8\_M}\, I_{5\_7\_M}\, I_{4\_5\_M}\, I_{4\_6\_M}\, I_{6\_9\_M}\, I_{8\_9\_M}\right]$$

For detection of any abnormal condition in the WSCC 9-bus system, as in Fig. 7, the voltage and current violations at each bus and transmission line are measured by measuring voltage violations and *CR* by using Eqs. (5) and (6), respectively.

During LLL fault in L_{4-5} under stressed system condition for WSCC 9-bus system, measured line current matrix for Area-1 and Area-2 is obtained referred from Eq. (7)

$$I_{A\_1\_M} = \left[\, I_{7\_8\_M}\;\; I_{5\_7\_M}\;\; I_{4\_5\_M} \,\right]$$

$$I_{A\_2\_M} = \left[\, I_{4\_6\_M}\;\; I_{6\_9\_M}\;\; I_{8\_9\_M} \,\right]$$

where$I_{A_1_M}$ and $I_{A\_2\_M}$ are the measured line current matrix for Area-1 and Area-2, respectively.

The area current ratio (ACR) for each area for the WSCC 9-bus system is calculated from Eq. (8) and represented as.

$$\mathrm{ACR}_{A\_1} = \frac{\max(I_{A\_1\_M})}{\max(I_{A\_1\_ST})} = \frac{I_{4\_5\_M}}{I_{4\_5\_ST}} \&$$

$$\mathrm{ACR}_{A\_2} = \frac{\max\left(I_{A\_2\_M}\right)}{\max\left(I_{A\_2\_ST}\right)} = \frac{I_{4\_6\_M}}{I_{8\_9\_ST}}$$

For analysis purposes the $\mathrm{ACR_{TH}}$ is considered as 1 for WSCC 9-bus system. The ACR_{A_1} and ACR_{A_2} both are found to be higher than the threshold value ACR_{TH}. Thus, both areas designated in Fig. 7 are considered under abnormal operating areas (Table 3).

The maximum current is found to be flowing through L_{4-5} in Area-I and in L_{4-6} in Area-II. Thus, the vulnerable buses

Table 3 V_{i_ST} and $I_{i\_j\_ST}$ of New England 39-bus system

Area-I		Area-II		Area-III	
Bus (i)	V_{i_ST} (PU)	Bus (i)	V_{i_ST} (PU)	Bus (i)	V_{i_ST} (PU)
1	1.14	4	0.98	15	0.953
2	1.08	5	0.97	16	0.94
3	1.024	6	0.972	19	0.93
9	1.093	7	0.96	20	0.951
17	0.97	8	0.954	21	0.931
18	1.055	10	0.953	22	0.93
25	1.11	11	0.951	23	0.935
26	1.12	12	0.96	24	0.99
27	0.96	13	0.94	33	1.01
28	1.14	14	0.98	34	1.12
29	1.12	31	0.991	35	0.998
30	0.97	32	1.008	36	0.991
37	1.01				
38	0.99				
39	1.14				
Line (i–j) L_{i-j}	$I_{i\_j\_ST}$ (PU)	Line L_{i-j}	$I_{i\_j\_ST}$ (PU)	Line L_{i-j}	$I_{i\_j\_ST}$ (PU)
L_{1-2}	0.966	L_{4-5}	1.597	L_{14-15}	0.8816
L_{1-39}	0.931	L_{4-14}	1.633	L_{15-16}	1.605
L_{2-3}	4.29	L_{5-6}	3.156	L_{16-19}	3.742
L_{2-25}	0.983	L_{5-8}	1.669	L_{16-21}	3.606
L_{3-4}	2.001	L_{6-7}	4.402	L_{16-24}	1.218
L_{3-18}	1.665	L_{6-11}	1.8	L_{21-22}	3.606
L_{8-9}	3.203	L_{7-8}	1.277	L_{22-23}	1.177
L_{9-39}	2.684	L_{10-11}	1.961	L_{23-24}	2.615
L_{17-18}	1.043	L_{10-13}	1.934		
L_{17-27}	3.412	L_{13-14}	2.142		
L_{25-26}	3.24	L_{16-17}	4.813		
L_{26-27}	2.732				
L_{26-28}	1.81				
L_{26-29}	0.722				
L_{28-29}	0.8934				

are identified as bus 4 in Area-I and bus 6 in Area-II. As soon as the vulnerable buses (bus 4 and bus 6) are identified, the power flow direction at both ends of lines L_{4-5}, $L_{4-6,}$ and L_{6-9} are compared.

Table 4 represents the bus voltage, line current violations, and abnormal operating area detection.

The equivalent circuit of WSCC 9-bus system for a LLL fault in L_{4_5} with stressed system conditions is shown in Fig. 11. Z_{4_F} and Z_{5_F} are the impedance of the line to the fault point from terminal *4* and *5*. V_F is the voltage at the fault point and Z_F is the fault impedance. The current I_{4_F} in section L_{4-5} from bus *4* and current I_{5_F} in section L_{4-5} from bus 5 is calculated from Eq. (10) and (13), respectively.

$$I_{4\_F} = \frac{V_4 - V_F}{Z_{4\_F} + Z_F} \&$$

$$I_{5\_F} = \frac{V_5 - V_F}{Z_{5\_F} + Z_F}$$

The phase angle difference δ_{vi_4} and δ_{vi_5} can be computed by referring Eq. (11) and (14), respectively.

$$\delta_{vi\_4} = \arg\left(\frac{I_{4\_F}}{V_4}\right) \&$$

$$\delta_{vi\_5} = \arg\left(\frac{I_{5\_F}}{V_5}\right)$$

The value of δ_{vi_4} and δ_{vi_5} are computed referring to Eqs. (12) and (15), respectively.

Table 4 ΔV, CR, ACR and Abnormal Operating Area (AOA) Detection for fault in L_{4-5} with stressed system condition in WSCC 9-bus System

Area	Bus (i)	V_{i_M} (PU)	ΔV	Is $\Delta V > 5\%$(Y/N)	Line L_{i-j}	$I_{i\_j\_M}$ (PU)	CR	Abnormal Condition	ACR	AOA
Area-I	2	0.8931	12.86	Y	L_{7-8}	0.723	2.73	Y	9.07	Y
	5	0.1528	84.28	Y	L_{5-7}	1.165	3.65	Y		
	7	0.6438	35.87	Y	L_{4-5}	3.602	9.07	Y		
	1	0.6524	37.26	Y						
	4	0.05538	94.44	Y						
Area-II	3	0.3138	69.38	N	L_{4-6}	0.5428	2.53	Y	1.95	Y
	6	0.1431	85.50	Y	L_{6-9}	0.5706	2.04	Y		
	8	0.4055	59.20	Y	L_{8-9}	0.5152	1.74	Y		
	9	0.3138	68.74	Y						

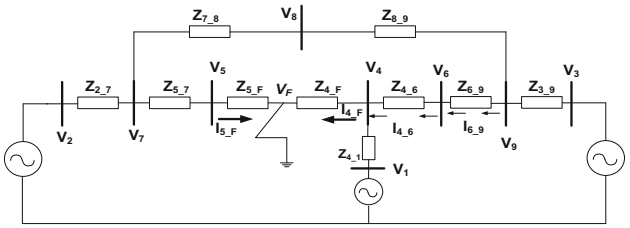

Fig. 11 Equivalent Circuit of WSCC 9-bus system for LLL fault in L_{4_5} with stressed system condition

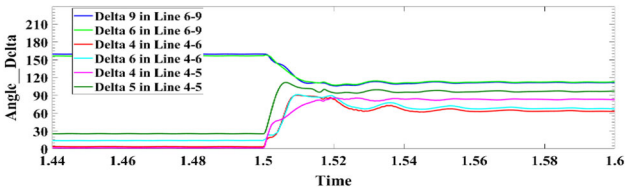

Fig. 12 Comparison of δ_{vi} for both ends of L_{6-9}, $L_{4-6,}$ and L_{4-5} for single fault with stressed system condition in WSCC 9-bus system

$$\delta_{vi\_4} = arg\left(\frac{V_4 - V_F}{(Z_{4\_F} + Z_F) * V_4}\right) \quad \& \delta_{vi\_5} = \arg\left(\frac{V_5 - V_F}{(Z_{5\_F} + Z_F) * V_5}\right).$$

The angular difference between terminal δ_{vi_4} and δ_{vi_5} is in the opposite range for the fault between section L_{4_5} and it is represented in Fig. 12.

Similarly, δ_{vi_6} and δ_{vi_9} for L_{6-9} and δ_{vi_4} and δ_{vi_6} are computed for L_{4_6} referring to Eqs. (12) and (15).

$$\delta_{vi\_6} = \arg\left(\frac{V_9 - V_6}{Z_{6\_9} * V_6}\right), \ \delta_{vi\_9} = \arg\left(\frac{V_9 - V_6}{Z_{6\_9} * V_9}\right)$$

$$\delta_{vi\_4} = \arg\left(\frac{V_6 - V_4}{Z_{6\_4} * V_4}\right), \ \delta_{vi\_6} = \arg\left(\frac{V_6 - V_4}{Z_{6\_4} * V_6}\right)$$

In Fig. 12, the angle δ_{vi} is compared for L_{6-9}, $L_{4-6,}$ and L_{4-5} and it is clear that after the fault event, δ_{vi} at line ends of L_{6-9} and L_{4-5} is in the same range. It means the power flow direction at both the terminals in $L_{6-9}$and L_{4-6} remains the same. Thus, no fault is there in between L_{6-9} and L_{4-6}, respectively. Angle δ_{vi} is also shown in Fig. 12 for both line ends of L_{4-5}. In this line, after the fault event, angle δ_{vi} for terminal 4 is in the opposite range with respect to terminal 6. This represents a fault in line L_{4-5}.

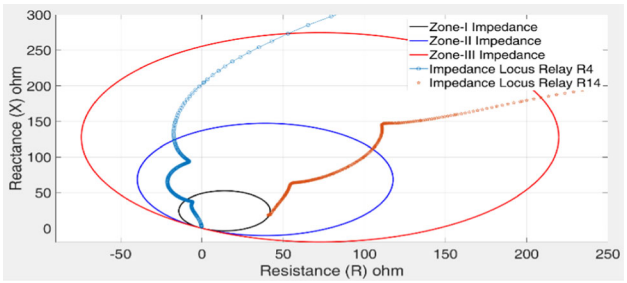

Fig. 13 MHO Relay R_4 and R_{14} characteristic for fault in L_{4-14} under stressed condition in New England 39-bus system

Similarly, for a single fault with stressed system conditions in New England 39-bus test system, a LLL fault is applied at 10% line length of L_{4-14} from bus 4 at 0.2 s in area-II. Additionally, stressed system condition is created in Area-I of the system by increasing the load at bus-27, bus-28, and bus-16, respectively, to 1.5 times their rated value and switching off the L_{2-3} and alternator at bus-37.

For this fault, Fig. 13 shows that conventional distance relays R_4 and R_{14} placed in L_{4-14}. It is observed that the impedance trajectory is obtained in two different zones, i.e., R_4 operates in zone-I and R_{14} operates in zone-II and thus initiate asynchronous tripping. Also, due to fault in Area-II (L_{4-14}) and stressed conditions in Area-I, R_{17} observes a reduced impedance under the zone-III and mal-operates during this stressed condition as shown in Fig. 14. The proposed SIPS enables the synchronous operation of relays R_4 and R_{14} at either end of line and blocks the undesirable operation of relay R_{17}.

Table 5 ΔV, CR, ACR and AOA Detection for single fault with stressed system condition in New England 39-bus system

Area	Bus (i)	V_{i_M} (PU)	ΔV	Is $\Delta V > 5\%$(Y/N)	Line L_{i-j}	$I_{i\_j\_M}$ (PU)	CR	Abnormal Condition	ACR	AOA
Area-I	1	0.926	19.47	Y	L_{1-2}	1.29	1.231	N	1.44	N
	2	0.952	13.7	Y	L_{1-39}	1.851	1.946	Y		
	3	0.222	81.93	Y	L_{2-3}	0	0	N		
	9	0.6605	41.99	Y	L_{2-25}	2.637	2.684	Y		
	17	0.3688	62.12	Y	L_{3-4}	5.152	3.131	Y		
	18	0.3258	71.35	Y	L_{3-18}	4.945	3.716	Y		
	25	0.8778	22.23	Y	L_{8-9}	5.338	1.66	Y		
	26	0.7162	37.33	Y	L_{9-39}	5.14	1.917	Y		
	27	0.3435	64.19	Y	L_{17-18}	2.401	5.979	Y		
	28	0.8586	26.3	Y	L_{17-27}	2.573	1.424	N		
	29	0.9018	21.26	Y	L_{25-26}	2.723	0.837	N		
	30	0.2954	74.56	Y	L_{26-27}	5.075	1.759	Y		
	37	0	100	Y	L_{26-28}	1.482	0.666	N		
	38	0.1517	84.47	Y	L_{26-29}	1.103	1.180	Y		
	39	0.8789	22.35	Y	L_{28-29}	1.369	1.544	Y		
Area-II	4	0.08167	97.82	Y	L_{4-5}	5.685	5.194	Y	2.31	Y
	5	0.1725	86.06	Y	L_{4-14}	10.34	8.756	Y		
	6	0.1852	77.94	Y	L_{5-6}	3.302	1.628	Y		
	7	0.1815	78.76	Y	L_{5-8}	3.118	2.005	Y		
	8	0.1805	79.07	Y	L_{6-7}	2.285	0.434	N		
	10	0.1318	86.89	Y	L_{6-11}	1.987	0.216	N		
	11	0.1916	74.92	Y	L_{7-8}	2.186	1.454	N		
	12	0.191	75.32	Y	L_{10-11}	2.408	0.757	N		
	13	0.1865	75.52	Y	L_{10-13}	2.801	1.246	N		
	14	0.0754	89.46	Y	L_{13-14}	4.886	1.418	N		
	31	0.1072	87.54	Y	L_{16-17}	3.302	0.567	N		
	32	0.5852	37.73	Y						
Area-III	15	0.2514	72.89	Y	L_{14-15}	6.963	7.236	Y	1.70	N
	16	0.4427	51.86	Y	L_{15-16}	7.125	4.072	Y		
	19	0.5574	39.33	Y	L_{16-19}	4.6	1.189	N		
	20	0.5761	39.8	Y	L_{16-21}	3.179	0.844	N		
	21	0.5522	39.66	Y	L_{16-24}	1.631	1.440	N		
	22	0.6656	27.56	Y	L_{21-22}	3.179	0.844	N		
	23	0.669	27.58	Y	L_{22-23}	0.252	0.264	N		
	24	0.474	56.73	Y	L_{23-24}	2.286	0.839	N		
	33	0.4218	58.23	Y						
	34	0.8958	20.45	Y						
	35	0.13	75.31	Y						
	36	0.117	84.3	Y						

Table 5 represents the bus voltage, line current violations, and abnormal operating area detection. For analysis purpose, the ACR_{TH} is considered 2 for New England 39-bus system. The ACR is higher than ACR_{TH} for Area-II only; thus, Area-II is considered as an abnormal area. In Area-II, the CR of L_{4-14} is highest, so the angle δ_{vi} of both ends of line connected to bus-4 and bus-14 are checked to find the faulted line. Figure 15 shows the angle δ_{vi} at bus-4 and bus-14, respectively. It is visible that after the fault event, the angle δ_{vi} for L_{4-14} is opposite for both line end terminals, i.e., bus-4 angle

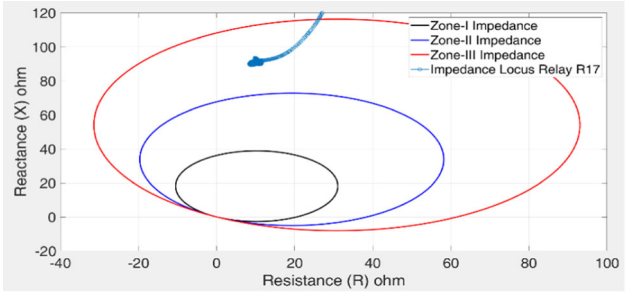

Fig. 14 MHO Relay R_{17} characteristic fault in $L_{4–14}$ under stressed condition in New England 39-bus system

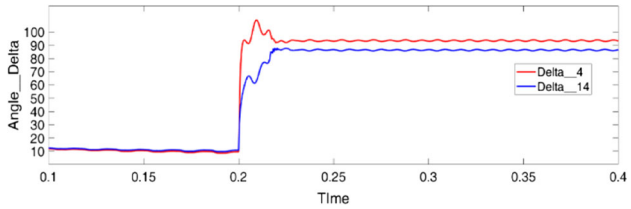

Fig. 15 Comparison of δ_{vi} for both ends of $L_{4–14}$ in New England 39-bus system

δ_{vi} is higher than 90° while bus-14 angle δ_{vi} is lower than 90°, and thus, $L_{4–14}$ is considered as a faulty line. The proposed algorithm successfully initiates the synchronous tripping at either end of $L_{4–14}$ as well as blocks the mal-operation of relay R_{17} as no fault is detected in area-I.

(b) Distance relay performance with proposed SIPS during Fault at multiple locations

For multi-location faults on WSCC 9-bus system, one LLL fault is applied at 10% of $L_{4–5}$ from bus-4 in Area-I and another LLL fault is applied at 10% line length of $L_{6–9}$ from bus 9 at 1.5 s.

During multi-location faults, conventional distance relay R_1 observes an impedance trajectory under zone-I and R_3 observes an impedance trajectory under zone-II as shown in Fig. 16 for fault in $L_{4–5}$. Similarly, the relay R_6 observes an impedance trajectory under zone-I and relay R_9 observes the impedance trajectory in zone-II as shown in Fig. 17. In both lines, the conventional approach initiates asynchronous tripping of relays at either end of lines. Also, due to multi-location faults, relay R_3 observes an impedance under its zone-I as shown in Fig. 18, and may mal-operate. The methods discussed in [9–13] may provide the accurate location of faults but will not be able to provide the synchronous tripping at either ends of lines.

Proposed SIPS accurately identifies the multi-location faults and blocks the tripping of healthy lines. For proposed SIPS, firstly violations of bus voltages and line current are observed and presented in Table 6.

Table 6 shows that the violations are observed, and the system is considered to be in an abnormal state. The calculated *ACR* is higher than 1 for both areas. The maximum current is observed to be flowing through $L_{4–5}$ in Area-I and in $L_{4–6}$ in Area-II. Thus, the vulnerable buses are identified as bus 4 in Area-I and bus 6 in Area-II. Figure 19 shows the equivalent circuit of WSCC 9-bus system during multi-location fault condition. The power flow direction for $L_{4–5}$, $L_{4–6}$, and $L_{6–9}$ is presented in Fig. 19.

The power flow direction at both ends of $L_{4–5}$, $L_{4–6}$, and $L_{6–9}$ is compared as in Fig. 20 by monitoring change of angle δ_{vi}. In these lines, after the fault events, angle δ_{vi} is opposite at both line end terminals for $L_{4–5}$ and $L_{6–9}$. It means the power flow direction at both the terminals in $L_{4–5}$ and $L_{6–9}$ is not the same and both lines are considered faulty lines. However, the δ_{vi} as found in the same range for both ends of $L_{4–6}$ which shows no fault in $L_{4–6}$.

Due to multi-location faults, relay R_2 also observes an impedance under its zone-II as shown in Fig. 18. The conventional algorithm observes this condition as a fault and may trip relay R_2, but the δ_{vi} comparison presented in Fig. 20 shows no fault in $L_{4–6}$ and the proposed algorithm blocks the relay R_2 to stop the unnecessary tripping.

Similarly, for multi-location fault scenarios in the New England 39-bus system shown in Fig. 8, a LLL fault is applied at the 10% line length of $L_{4–14}$ from bus-4 in Area-II and another LLL fault is applied at 10% line length of $L_{23–24}$ from bus-23 at 0.2 s.

During the event, conventional distance relay R_4 sees an impedance trajectory in zone-I and R_{14} sees the impedance trajectory in zone-II as shown in Fig. 21. Similarly, the relay R_{23} sees an impedance trajectory under zone-I and relay R_{24} sees the impedance trajectory in zone-II as shown in Fig. 22. In both lines, the conventional approach initiates asynchronous tripping. Relay R_{16} also sees a reduction in impedance as shown in Fig. 23 and experience a fault in its zone-II enabling conventional protection scheme to trip R_{16}.

For enabling synchronous tripping and blocking the mal-operation of relay R_{16}, proposed algorithm first detects the bus voltage and line current violations as presented in Table 7.

As violations are observed, the system is considered to be in an abnormal state. The calculated ACR is higher than ACR_{TH} for Area-II and Area-III, respectively. The maximum current is found to be flowing through $L_{4–14}$ in Area-II and in $L_{16–24}$ in Area-III. Thus, the vulnerable buses are identified as bus-4 in Area-I and bus-24 in Area-III, respectively.

The power flow direction at both ends of $L_{4–14}$, $L_{14–13}$, and $L_{14–15}$ is compared as in Fig. 24 by analyzing the angle δ_{vi}. In $L_{4–14}$, after the fault event, angle δ_{vi} for $L_{4–14}$ is opposite for both line end terminals, i.e., for bus-4 angle δ_{vi} is higher than 90° while bus-14 angle δ_{vi} is lower than 90°, thus

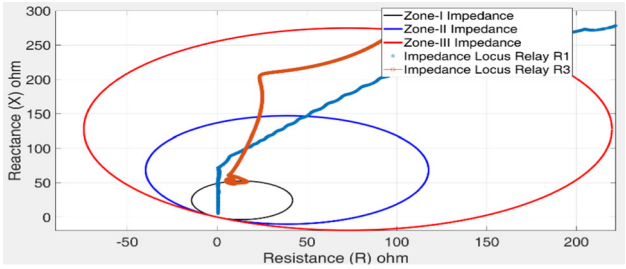

Fig. 16 MHO Relay R_1 and R_3 Characteristic for multi-location faults in WSCC 9-bus system

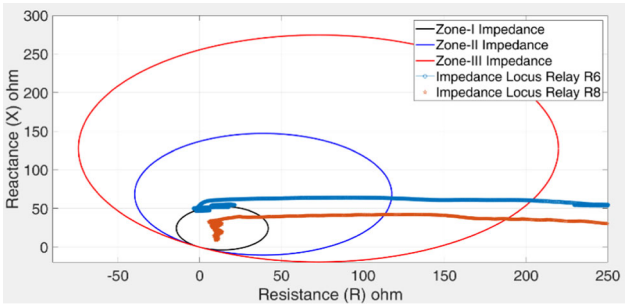

Fig. 17 MHO Relay R_6 and R_8 Characteristic for multi-location faults in WSCC 9-bus system

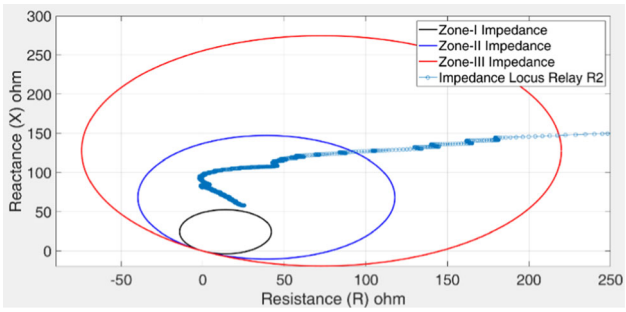

Fig. 18 MHO Relay R_2 Characteristic for multi-location faults in WSCC 9-bus system

$L_{4–14}$ is considered as the faulty line. Similarly, the power flow direction at both ends of $L_{23–24}$ and $L_{16–24}$ is compared. Figure 24 also shows that δ_{vi} for $L_{23–24}$ is opposite for both line end terminals and it is also considered as the faulty line. The proposed algorithm ensures a fault at multi-location, i.e., in $L_{23–24}$ and $L_{4–14}$, respectively, and initiates synchronous tripping of relays at either end of the line. Also, from the proposed algorithm, no fault is observed in lines connected to bus-16; thus, the mal-operation of Relay R_{16} is blocked.

(c) Distance relay performance in higher operating zones with proposed SIPS during stressed conditions

The performance of distance relay in the higher operating zone is assisted through proposed SIPS in WSCC 9-bus system and New England 39-bus system.

To test the performance of the relay in the WSCC 9-bus system, Area-I is stressed by similar conditions imposed in section (a), and Area-II is stressed by switching off its generators at 1 s. With the stressed conditions, MHO relay R_{11} at bus-8 observes an impedance trajectory under zone-III as presented in Fig. 25. The conventional algorithm identifies it as a fault in zone-III of relay R_{11} and may initiate the unwanted relay tripping. The methods [9–13] discussed in the literature are not providing the coordination of backup distance protection in higher operating zones. Thus, these methods will also fail to stop the distance relay mal-operation during stressed conditions.

The proposed algorithm restricts the operation of distance relay in higher operating zones due to stressed condition. First, the violations in voltage and current are observed and the system is abnormality is detected. The violations of bus voltages and line current are presented in Table 8.

The ACR is also calculated for further verification of abnormal areas, and it is found to be higher than 1.5 for both areas. The CR is higher than 1 in $L_{7–8}$ and $L_{5–7}$ in Area-I and $L_{4–6}$ in Area-II, respectively. Thus, the vulnerable bus is identified as bus 7 in Area-I, further δ_{vi} is compared for both ends of lines connected to bus 7. In Area-II, $L_{6–9,}$ and $L_{8–9}$ both CR is found to be less than 1, thus δ_{vi} is compared only for both ends of $L_{4–6}$. Figure 26 shows the equivalent circuit of WSCC 9-bus system during stressed system conditions. The power flow direction for $L_{4–6}$, $L_{7–8,}$ and $L_{5–7}$ is also presented in Fig. 26, respectively. In Fig. 27, the angle δ_{vi} is represented for $L_{4–6}$, $L_{7–8,}$ and $L_{5–7}$. In these lines, after the generator tripping event, the angle δ_{vi} for all the lines are obtained to be in the same range for both line end terminals. It means that the power flow directions at both the terminals in $L_{4–6}$, $L_{7–8,}$ and $L_{5–7}$ are the same and no lines are faulty.

As no fault is detected in any of the transmission lines in the system, the distance relay operation in higher operating zone is blocked. This blocking operation restricts unnecessary tripping and enhances the system's resilience.

The performance of proposed method is also tested on New England 39-bus test system for coordination of distance relay higher operating zone during stressed condition.

The stressed condition in Area-I of New England 39-bus system of Fig. 8 is created by similar conditions imposed in section (a). Area-II is stressed by switching off $L_{13–14}$ and $L_{9–39}$ at 0.2 s. Due to imposed stressed conditions, MHO relay R_3 sees an impedance trajectory under zone-III as shown in Fig. 28. The conventional algorithm shows a fault in zone-III of relay $R_3$and initiates the unwanted tripping.

With the proposed algorithm, the unwanted tripping of relay R_3may be blocked. The proposed method measures the

Table 6 ΔV, CR, ACR and AOA Detection for fault at Multiple Locations in WSCC 9-bus system

Area	Bus (i)	V_{i_M} (PU)	ΔV	Is $\Delta V > 5\%$(Y/N)	Line L_{ij}	$I_{i\_j\_M}$ (PU)	CR	Abnormal condition	ACR	AOA
Area-I	2	0.8933	12.84	Y	L_{7-8}	0.988	3.732	N	7.488	Y
	5	0.1308	86.54	Y	L_{5-7}	0.9878	3.098	Y		
	7	0.6607	34.19	Y	L_{4-5}	2.973	7.488	Y		
	1	0.5157	50.41	Y						
	4	0.0464	95.34	Y						
Area-II	3	0.6127	40.22	N	L_{4-6}	3.41	15.823	Y	14.12	Y
	6	0.1289	86.94	Y	L_{6-9}	4.16	14.622	Y		
	8	0.3422	65.57	Y	L_{8-9}	1.11	3.769	Y		
	9	0.1263	87.42	Y						

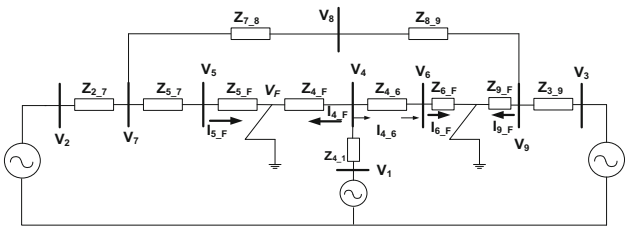

Fig. 19 Equivalent Circuit of WSCC 9-bus system for multi-location faults

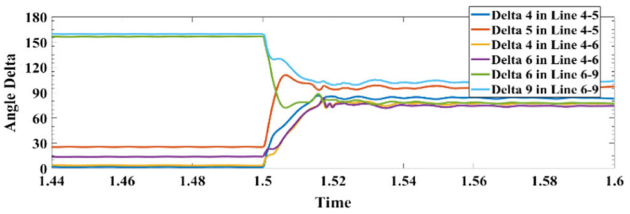

Fig. 20 Comparison of δ_{vi} for both ends of L_{4-5}, L_{4-6} and L_{6-9} for multiple fault location in WSCC 9-bus system

violations of bus voltages and line current as presented in Table 9.

During stressed condition, no violations in current and voltage are observed, and the system is considered to be in normal state. The *ACR* is also calculated for further verification of abnormal areas, and it is found to be lower than 1.5 for all the areas. Thus, the proposed algorithm assists the operation of distance relay in higher operating zones and blocks unwanted tripping.

5.3 Practical Implementation of Proposed SIPS on Typhoon HIL

The proposed method is also tested in the real-time platform to validate it for practical implementation. Real-time emulation allows visualization of the actual dynamics under the practical scenario. For real-time implementation, Typhoon

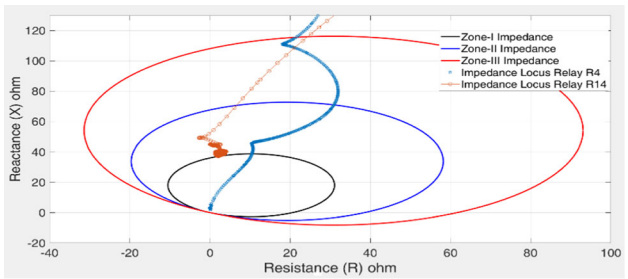

Fig. 21 MHO Relay R_4 and R_{14} characteristic for multi-location fault in New England 39-bus system

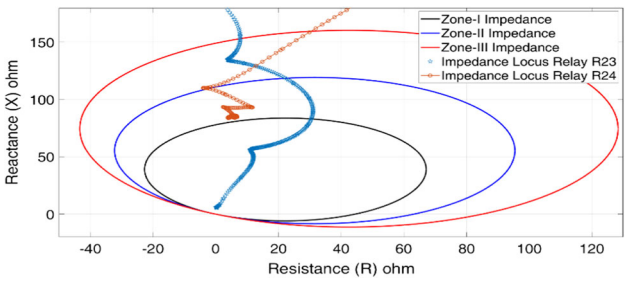

Fig. 22 MHO Relay R_{23} and R_{24} characteristic for multi-location faults in New England 39-bus system

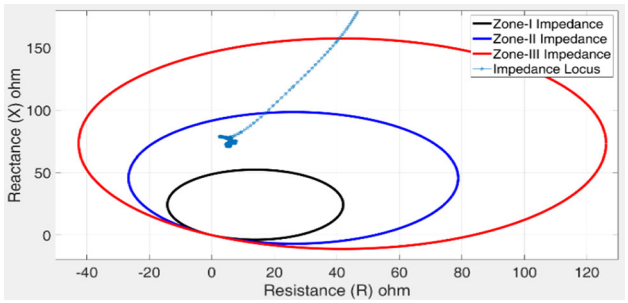

Fig. 23 MHO Relay R_{16} characteristic for multi-location faults in New England 39-bus system

Table 7 ΔV, CR, ACR and AOA Detection for multi-location faults in New England 39-bus system

Area	Bus (i)	V_{i_M} (PU)	ΔV	Is $V > 5\%$(Y/N)	Line L_{ij}	$I_{i\_j\_M}$ (PU)	CR	Abnormal condition	ACR	AOA
Area-I	1	0.6134	46.19	Y	$L_{1–2}$	0.927	0.96	N	1.47	N
	2	0.5068	53.07	Y	$L_{1–39}$	0.4131	0.44	N		
	3	0.0.31	96.97	Y	$L_{2–3}$	6.508	1.51	N		
	9	0.4844	55.68	Y	$L_{2–25}$	2.337	2.377	Y		
	17	0.1029	89.39	Y	$L_{3–4}$	6.005	3	Y		
	18	0.2696	74.44	Y	$L_{3–18}$	0.7788	0.467	N		
	25	0.5482	50.61	Y	$L_{8–9}$	3.657	1.141	N		
	26	0.5002	55.33	Y	$L_{9–39}$	3.495	1.30	N		
	27	0.1272	86.75	Y	$L_{17–18}$	0.931	0.892	N		
	28	0.8121	28.76	Y	$L_{17–27}$	3.521	1.031	N		
	29	0.8621	23.02	Y	$L_{25–26}$	1.549	0.478	N		
	30	0.1442	85.13	Y	$L_{26–27}$	3.721	1.36	N		
	37	0.2165	78.56	Y	$L_{26–28}$	1.415	0.781	N		
	38	0.2914	70.56	Y	$L_{26–29}$	1.203	1.666	Y		
	39	0.8	29.82	Y	$L_{28–29}$	1.41	1.58	Y		
Area-II	4	0.0662	93.24	Y	$L_{4–5}$	4.708	2.948	Y	2.82	Y
	5	0.1925	80.15	Y	$L_{4–14}$	10.47	6.411	Y		
	6	0.2352	75.80	Y	$L_{5–6}$	2.845	0.901	N		
	7	0.1815	81.09	Y	$L_{5–8}$	2.184	1.308	Y		
	8	0.1805	81.07	Y	$L_{6–7}$	1.468	0.33	N		
	10	0.1219	87.20	Y	$L_{6–11}$	1.965	1.091	N		
	11	0.1916	79.85	Y	$L_{7–8}$	1.379	1.079	Y		
	12	0.191	80.10	Y	$L_{10–11}$	2.183	1.113	N		
	13	0.1865	80.15	Y	$L_{10–13}$	3.216	1.66	N		
	14	0.0754	92.30	Y	$L_{13–14}$	5.379	2.511	Y		
	31	0.1072	89.18	Y	$L_{16–17}$	4.432	0.920	N		
	32	0.5935	41.12	Y						
Area-III	15	0.1505	84.20	Y	$L_{14–15}$	3.008	3.41	Y	2.892	Y
	16	0.4427	52.90	Y	$L_{15–16}$	3.091	1.92	Y		
	19	0.4901	47.30	Y	$L_{16–19}$	5.658	1.51	N		
	20	0.4911	48.35	Y	$L_{16–21}$	1.764	0.489	N		
	21	0.2285	75.45	Y	$L_{16–24}$	6.229	5.11	Y		
	22	0.3362	63.84	Y	$L_{21–22}$	1.764	0.489	N		
	23	0.3181	65.97	Y	$L_{22–23}$	3.497	2.97	Y		
	24	0.4605	53.48	Y	$L_{23–24}$	6.202	2.371	Y		
	33	0.4218	58.23	Y						
	34	0.8595	23.25	Y						
	35	0.1045	89.52	Y						
	36	0.1079	89.11	Y						

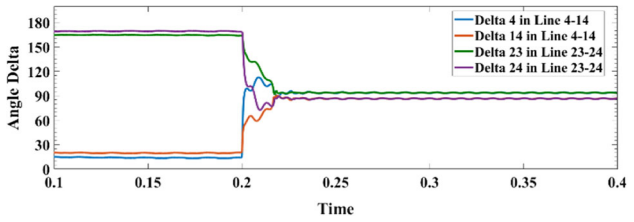

Fig. 24 Comparison of angle δ_{vi} for $L_{4–14}$ and $L_{23–24}$ in New England 39-bus system

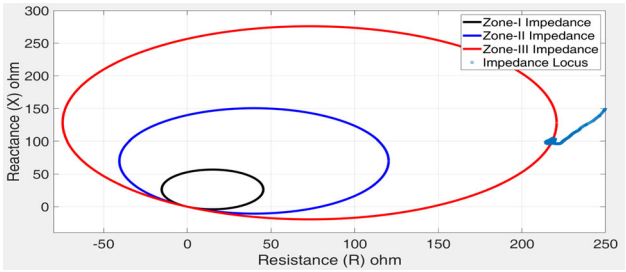

Fig. 25 MHO Relay R_8 Characteristic for L_{7-8} in WSCC 9–bus system for multi-area stressed conditions

HIL 602 + with configuration 5, hardware in loop digital emulator is used. The four-bus test system shown in Fig. 4a is designed and run in Typhoon HIL as presented in Fig. 29. The data obtained from the real-time emulator are utilized to run the proposed algorithm.

The steady-state bus voltage and line current phasors of the 4-bus test system obtained from Typhoon HIL are represented in Table 10.

This algorithm is mainly focused to accurately identify the multi-location faults and multi-area stressed conditions. For this purpose, the proposed SIPS is validated through Typhoon HIL for the following two scenarios.

(a) Distance relay operation with proposed SIPS during multi-locations faults for Typhoon HIL-based 4-bus test system

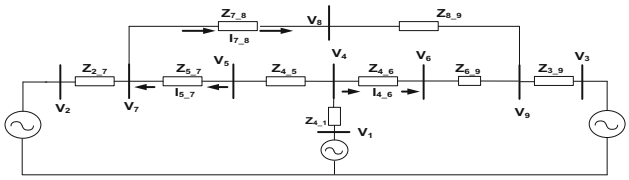

Fig. 26 Equivalent Circuit of WSCC 9-bus system for stressed system conditions

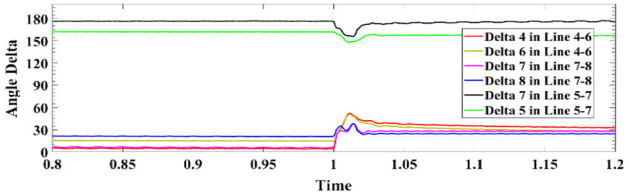

Fig. 27 Comparison of δ_{vi} for both ends of $L_{4–6}$, $L_{7–8,}$ and $L_{5–7}$ in WSCC 9-bus system

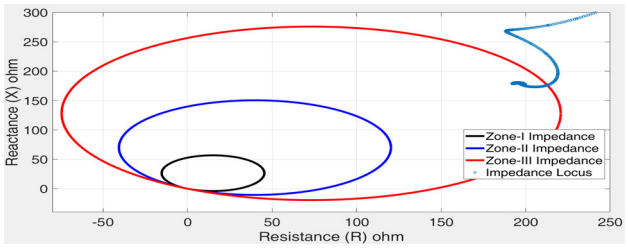

Fig. 28 MHO Relay R_3Characteristic for $L_{3–4}$ in New England 39-bus system for multi-area stressed conditions

For multi-location faults on 4-bus test system of Fig. 4a, one LLL fault is initiated at 70% line length of $L_{B–D}$ from bus-B in Area-I and another LLL fault is initiated at 70% of $L_{B–C}$ from bus-B in Area-II.

Table 11 shows that the violations are observed and the calculated ACR is higher than 1 for both areas. The power flow direction at both ends of $L_{B–C}$, and $L_{B–D}$ is compared

Table 8 ΔV, CR, ACR and AOA Detection for multi-area stressed condition in WSCC 9-bus system

Area	Bus (i)	V_{i_M} (PU)	ΔV	Is $\Delta V > 5\%$(Y/N)	Line L_{ij}	$I_{i\_j\_M}$ (PU)	CR	Abnormal condition	ACR	AOA
Area-I	2	0.9831	4.087	N	L_{78}	1.078	4.07	Y	2.71	Y
	5	0.9124	6.170	Y	L_{57}	0.3279	1.028	Y		
	7	0.9235	8.017	Y	L_{45}	0.3138	0.7904	N		
	1	0.994	4.423	N						
	4	0.933	6.381	Y						
Area-II	3				L_{46}	1.062	4.928	Y	3.73	Y
	6	0.913	10.926	Y	L_{69}	0.2084	0.7404	N		
	8	0.891	9.726	Y	L_{89}	0.2102	0.714	N		
	9	0.893	10.160	Y						

Table 9 ΔV, CR, ACR and AOA Detection for multi-area stressed condition in New England 39-bus system

Area	Bus (i)	V_{i_M} (PU)	ΔV	Is $\Delta V > 5\%$(Y/N)	Line L_{ij}	$I_{i\_j\_M}$ (PU)	CR	Abnormal condition	ACR	AOA
Area-I	1	1.14	1.08	Y	L_{1-2}	3.331	3.44	N	1.03	N
	2	1.08	1.07	N	L_{1-39}	2.523	2.70	N		
	3	1.024	0.98	N	L_{2-3}	6.346	1.47	N		
	9	1.093	1.017	Y	L_{2-25}	0.4475	0.45	Y		
	17	0.97	0.96	N	L_{3-4}	3.648	1.82	Y		
	18	1.055	0.97	Y	L_{3-18}	1.451	0.87	N		
	25	1.11	1.073	N	L_{8-9}	0.4258	0.13	N		
	26	1.12	0.98	Y	L_{9-39}	0	0	N		
	27	0.96	0.956	N	L_{17-18}	1.043	1	N		
	28	1.14	1.038	Y	L_{17-27}	2.521	0.709	N		
	29	1.12	1.061	Y	L_{25-26}	3.306	1.02	N		
	30	0.97	0.963	N	L_{26-27}	2.39	0.87	N		
	37	1.01	1.004	N	L_{26-28}	0.733	0.40	N		
	38	0.99	0.98	N	L_{26-29}	0.408	0.56	Y		
	39	1.14	1.132	N	L_{28-29}	1.464	1.63	Y		
Area-II	4	0.98	0.975	N	L_{4-5}	1.7	1.06	Y	0.86	N
	5	0.97	0.966	N	L_{4-14}	0.818	0.50	Y		
	6	0.972	0.961	N	L_{5-6}	1.893	0.599	N		
	7	0.96	0.956	N	L_{5-8}	2.007	1.202	N		
	8	0.954	0.967	N	L_{6-7}	2.299	0.522	N		
	10	0.953	0.953	N	L_{6-11}	3.817	2.12	N		
	11	0.951	0.952	N	L_{7-8}	0.979	0.766	N		
	12	0.96	0.96	N	L_{10-11}	2.816	1.436	N		
	13	0.94	0.939	N	L_{10-13}	1.395	0.721	Y		
	14	0.98	0.967	N	L_{13-14}	0	0	Y		
	31	0.991	0.990	N	L_{16-17}	2.722	0.566	N		
	32	1.008	0.984	N						
Area-III	15	0.953	0.949	N	L_{14-15}	0.8816	0.848	Y	1.02	N
	16	0.94	0.934	N	L_{15-16}	1.605	1.68	Y		
	19	0.93	0.93	N	L_{16-19}	3.742	1.015	Y		
	20	0.951	0.95	N	L_{16-21}	3.606	0.867	N		
	21	0.931	0.96	N	L_{16-24}	1.218	0.317	Y		
	22	0.93	0.931	N	L_{21-22}	3.606	0.867	N		
	23	0.935	0.933	N	L_{22-23}	1.177	0.669	Y		
	24	0.99	0.98	N	L_{23-24}	2.615	0.867	Y		
	33	1.01	0.997	N						
	34	1.12	0.998	Y						
	35	0.998	0.978	N						
	36	0.991	0.983	N						

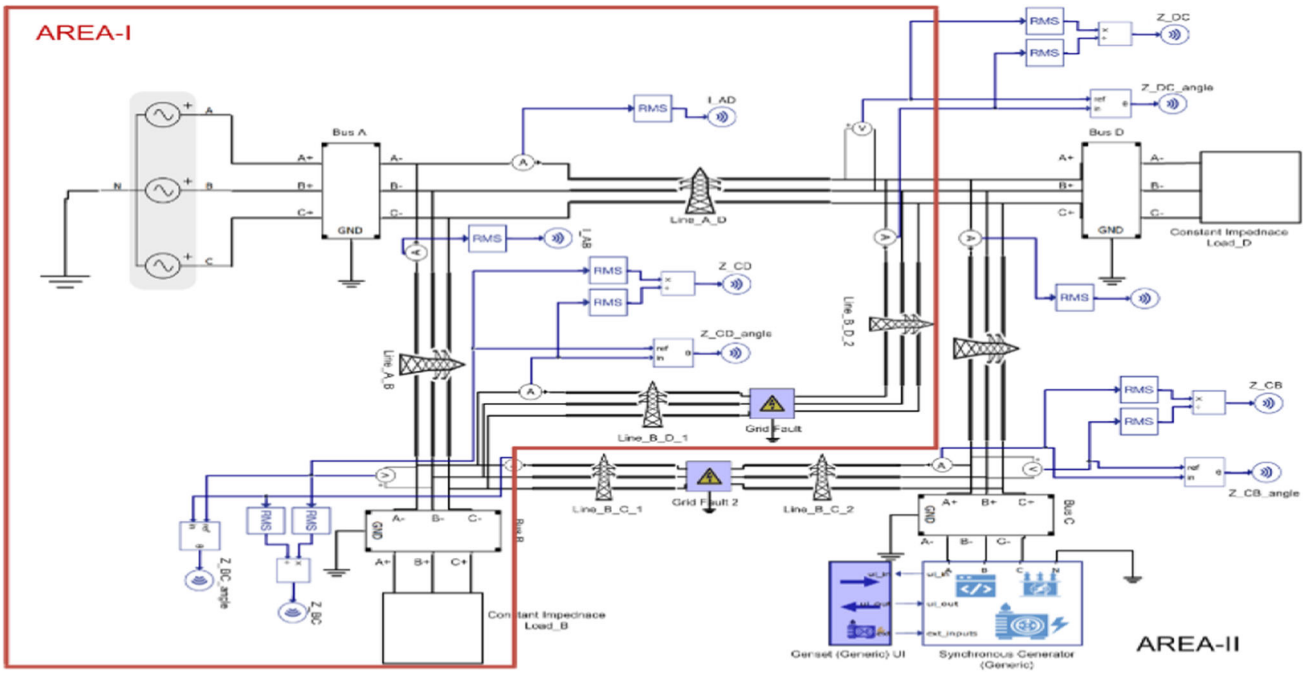

Fig. 29 4-bus test system in Typhoon HIL 602 +

Table 10 V_{i_ST} and $I_{i\_j\_ST}$ of 4-bus test system

Area	Bus (i)	V_{i_ST} (PU)	Line (i–j)	$I_{i\_j\_ST}$ (PU)
Area-I	A	1.001	$L_{A–D}$	0.2177
	B	0.9983	$L_{A–B}$	0.483
			$L_{B–D}$	0.055
Area-II	D	0.9968	$L_{B–C}$	0.1716
	C	1.0003	$L_{C–D}$	0.324

Table 11 ΔV, CR, ACR and AOA detection for multi-area stressed condition in 4-bus system with Typhoon HIL

Area	Bus (i)	V_{i_M} (PU)	ΔV	Is $\Delta V > 5\%$(Y/N)	Line L_{ij}	$I_{i\_j\_M}$ (PU)	CR	Abnormal condition	ACR	AOA
I	A	0.96	4.09	N	$L_{A–D}$	4.69	21.54	Y	9.92	Y
	B	0.302	69.7	Y	$L_{A–B}$	7.77	16.08	Y		
					$L_{B–D}$	4	72.77	Y		
II	D	0.242	76.2	Y	$L_{B–C}$	4	23.31	Y	16.7	Y
	C	0.558	44.2	Y	$L_{C–D}$	5.43	16.75	Y		

as in Fig. 30 by monitoring the change of angle δ_{vi}. In these lines, after the fault events, the angle δ_{vi} is opposite at both line end terminals for $L_{B–C}$ and $L_{B–D}$ and thus initiate synchronous tripping of both lines.

b) Distance relay operation in higher operating zones with proposed SIPS during stressed conditions for Typhoon HIL-based 4-bus test system

To assess the distance relay performance with proposed scheme in higher operating zones during stressed conditions, the load of the network is increased to double capacity and $L_{C–D}$ is switched off. The performance of R_5 is tested by initiating a tripping of $L_{C–D}$. It.

During stressed condition, the higher operating zone of distance relay R_5, i.e., zone-III observes an impedance trajectory under its characteristic as shown in Fig. 31 initiates mal-operation.

Table 12 shows that the violations are observed and calculated ACR is higher than 1 for Area-II. The power flow direction at both ends of $L_{B–D}$, is compared as in Fig. 32 by monitoring change of angle δ_{vi}. δ_{vi} comparison in Fig. 32

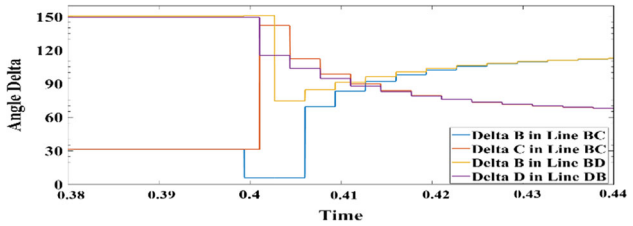

Fig. 30 Comparison of δ_{vi} for both ends of L_{B-C} and L_{B-D} in 4-bus system

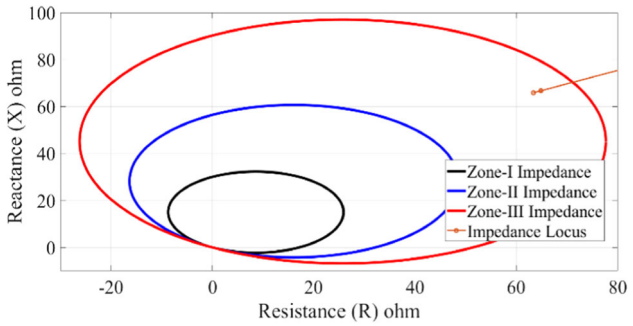

Fig. 31 MHO Relay R_5Characteristic for L_{B-D} in 4-bus test system

shows no fault in L_{B-D} and unwanted tripping of L_{B-D} in the higher operating zone is blocked.

5.4 Resistance indices-based resilience assessment

The resistance indices discussed in Sect. 4 are calculated in this section using Eqs. (19)–(21) for resilience assessment during HILF events based on all the conditions presented in Sect. 5.2 for both the considered network.

For WSCC 9-bus system, the resistance indices CLPP, ATCS, and APDA are calculated for the network as a whole. A similar analysis is adopted for New England 39-bus system but is restricted to area presented in Table 9 as in Sect. 5.1.

For scenario (a), the conventional protection scheme trips the L_{4-5}, $L_{4-6,}$ and L_{6-9} due to fault under stressed conditions and the load of bus 6 gets completely disconnected in WSCC 9-bus system. Similarly, in New England 39-bus system, the conventional scheme may trip relay R_{17} due to stressed network conditions. The proposed algorithm restricts the unnecessary tripping of L_{4-6} and L_{6-9} in WSCC

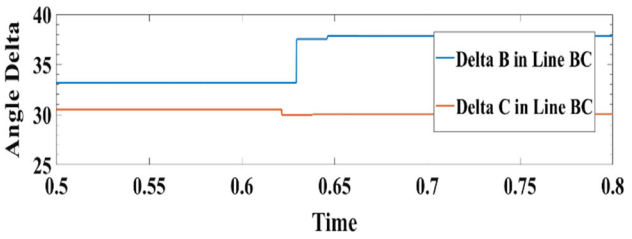

Fig. 32 Comparison of δ_{vi} for both ends of L_{B-C} in 4-bus system

9-bus system and similarly, blocks the operation of relay R_{17} in New England 39-bus system and resulting in improved resistance indices. With the proposed algorithm, for WSCC 9-bus system, the CLPP is zero, which means no loads are disconnected from the system. Also, the values of ATCS and APDA are improved with the proposed algorithm. Also, the improved values of CLPP and ATCS for Area-I of New England 39-bus system represent an enhancement in resilience during disaster.

For scenario (b) as in Sect. 5.1, the multi-location fault in L_{4-5} and L_{6-9} trips relay R_2 for WSCC 9-bus system and relay R_{16} in New England 39-bus system with conventional protection scheme. Tripping operation for 9-bus system disconnects the generator G-1 and load at bus 6 from the system. The *CLPP*, *ATCS*, and *APDA* with the conventional algorithm are represented in Table 9. The proposed algorithm stops the unwanted tripping of relays in both the networks and improves the resistance indices. The improved resistance indices for both WSCC 9-bus system and Area-III of New England 39-bus system are presented in Table 13.

Similarly, in scenario (c) as Sect. 5.1, the conventional protection scheme trips relay R_8 for WSCC 9-bus system and relay R_3 in Area-I of New England 39-bus system, due to multi-area stressed conditions. Due to the increase in load, the *APDA* is high that requires load shedding with both algorithms. But with the proposed algorithm, the increase in *ATCS* reduces the amount of load shedding compared to the conventional algorithm. The proposed algorithm improves the resistance indices and thus improves the resilience of the network.

The resistance indices also calculated using Eqs. (19)–(21) for conditions discussed in Sect. 5.3 for 4-bus test system,

Table 12 ΔV, CR, ACR and AOA Detection for multi-area stressed condition in 4-bus system with Typhoon HIL

Area	Bus (i)	V_{i_M} (PU)	ΔV	Is $\Delta V > 5\%$(Y/N)	Line L_{ij}	$I_{i\_j\_M}$ (PU)	CR	Abnormal Condition	ACR	AOA
I	A	1	0	N	L_{A-D}	0	0	N	0.416	N
	B	0.988	1.04	Y	L_{A-B}	1.23	2.54	N		
					L_{B-D}	1.159	21.07	Y		
II	D	0.968	2.88	Y	L_{B-C}	0	0	N	4.84	Y
	B	0.988	1.49	Y	L_{C-D}	0.511	1.57	N		

Table 13 Comparative analysis of conventional Protection Scheme and Proposed SIPS for resilience assessment

Indices	Fault at single location with stressed condition				Fault at multiple locations								Stressed system conditions							
	9-bus system		39-bus system (Area-I)		9-bus system		39-bus system (Area-III)		4-bus test system on Typhoon HIL				9-bus system		39-bus system (Area-I)		4-bus test system on Typhoon HIL			
	Conventional approach	Proposed SIPS	Conventional approach	Proposed SIPS	Conventional approach	Proposed SIPS	Conventional approach	Proposed SIPS	Conventional approach	Proposed SIPS			Conventional approach	Proposed SIPS	Conventional approach	Proposed SIPS	Conventional approach	Proposed SIPS		
CLPP	0.27797	0	0.043	0	0.27797	0	0.239	0.239	0.5	0			0	0	0.043	0	0	0		
ATCS (MVA)	343.96	443.96	483.38	683.38	353.58	553.58	18.1	268.1	50	100			443.96	663.96	483.38	683.38	100	150		
APDA (MW)	157	90	119	119	157	90	244	244	0	0			253	253	119	119	40	40		

validated in Typhoon HIL. For Sect. 5.3 (a), during multi-location faults in L_{B-C} and L_{B-D}, relay at bus-B mal-operate due to reduction in impedance and trips L_{A-B} and disconnect the load of bus-B from the existing system. The resistance indices with the conventional protection scheme and with the proposed scheme are presented in Table 13. Blocking the unwanted tripping of the relay at bus-B in L_{A-B} improves the resilience of the network.

Similarly, in scenario 5.3 (b), the conventional protection scheme trips relay R_5 for 4-bus test system, due to multi-area stressed conditions. The high amount of APDA due to an increase in load necessitates load shedding with both algorithms. But as compared to the conventional algorithm, the proposed approach results in less load shedding due to an increase in ATCS.

Hence, the resistance indices presented in Table 13 are calculated and compared for different abnormal conditions on WSCC 9-bus, New England 39-bus system, and 4-bus test system for conventional approach and proposed SIPS. These indices present a decline in CLPP to 0%, an increase in ATCS up to 140%, and a reduction in APDA up to 57% during different operating conditions for considered test systems. The improvement in indices represents an augmentation in resilience with the proposed protection scheme during HILF events.

5.5 Comparison of proposed SIPS with existing methods

In this section, a comparison between the proposed algorithm and existing algorithms is done and presented in Table 14.

All methods shown in the literature [9–13] are capable of finding the multi-location faults but the proposed algorithm has certain advantages based on the following points.

(a) Identification of stressed area: During HILF events, it is important to discriminate the stressed area from the faulty area. The proposed method and method represented in [13] are only capable to differentiate between a stressed system condition and multi-area fault identification.
(b) Measurement of resiliency indices: Proposed method is focused on the identification of multi-location faults and stressed conditions during a HILF event for resilience improvement of the network. No other method from the literature presents the improvement in the resilience of the system.
(c) Utilization of SIPS: In [15], the SIPS is proposed to restrict the overload caused by high wind generation due to the HILF event. Other than that, no literature is proposed for utilizing SIPS for restricting the cascaded outage due to HILF events.

Table 14 Comparison of Proposed Method with existing literature

Reference	Identification of stressed area	Measurement of resilience indices	Utilization of SIPS	PMUs location	Requirement of training and data sets
[9]	X	X	X	Optimum	Not required
[10]	X	X	X	All	Required
[11]	X	X	X	All	Required
[12]	X	X	X	All	Not required
[13]	↘	X	X	NA	Not required
[15]	X	X	↘	Optimum	Not required
Proposed	↘	↘	↘	Optimum	Not required

(d) PMUs location: The methods represented in [10–12] need PMU at all buses within a network. The proposed method requires the optimal PMU data for decision-making. This makes the proposed approach more practical and economical.
(e) Requirement of training and large data sets: The proposed method does not require any data sets and computational training compared to the soft computing-based method.

6 Conclusion

Robustness is an important feature of a resilient power system, and it can be increased by deploying suitable SIPS. This work proposed a SIPS to enhance the robustness of a resilient power system during HILF events such as multi-location faults and multi-area stressed system conditions. Proposed SIPS utilizes local and global data for accurate multi-location fault identification for synchronized distance relay tripping at either end of lines. Also, the proposed method restricts the distance relay operation in higher operating zones during no fault yet stressed system conditions. Under abnormal operating conditions, real-time data from PMUs are utilized to calculate ΔV and CR to identify the abnormality in the system. After the abnormality detection, the abnormal area and vulnerable buses are identified using the ACR. After the identification of vulnerable buses, the lines connected to these buses are tested for faulty conditions by comparing δ_{vi}, i.e., the phase angle between voltage and current of either end of the line. The synchronized operation of distance relay is supervised based on the comparison of this angle. Results show that the proposed method effectively detects multi-location faults and enables synchronized tripping of relays for such faults. The operation of backup distance relay in higher operating zones is assisted with the proposed method. Results show that the unwanted operation of the backup relay in zone-III is blocked if δ_{vi} is in the same range at either end of the line, hence increasing the robustness of the system. The proposed methodology has been tested through extensive case studies conducted on WSCC 9-bus and New England 39-bus systems and validated for a 4-bus test system developed on Typhoon HIL. The resistance indices CLPP, ATCS, and APDA are also calculated and compared for different abnormal conditions on WSCC 9-bus, New England 39-bus system, and Typhoon 4-bus test system for conventional approach and proposed SIPS. With the implementation of the proposed SIPS, the transmission capacity increases up to 140%, the load loss percent reduces up to 0%, and the active power deficiency is enhanced up to 57% during different operating conditions for considered test systems. It represents an augmentation in resilience with the proposed protection scheme during HILF events.

References

1. "Final Report on August 14, 2003 blackout in the United States and Canada," US- Canada Power System Outage Task Force, Canada (2004).
2. Report on Grid Disturbance on 30th and 31st July 2012. CERC, New Delhi (2012).
3. Rajalwal N, Ghosh D (2020) Recent trends in integrity protection of power system: A literature review. Int Trans Electrical Energy Syst. https://doi.org/10.1002/2050-7038.12523.
4. Soonee SK, Narasimhan SR, Nallarasan N, Rathour HK, Yadav G, Bhan S, Mali R (2015) Impact of very severe cyclone 'HudHud' on power system operation. In: Annual IEEE India Conference (INDICON). New Delhi, India
5. Henry D, Ramirez-Marquez JE (2016) On the impacts of power outages during Hurricane Sandy—a resilience-based analysis. Syst Eng 1(19):59–75
6. Lai LL, Zhang H, Mishra S, Ramasubramanian D, Lai C, Xu F (2012) Lessons learned from July 2012 Indian blackout. In: 9th IET International Conference on Advances in Power System Control, Operation and Management (APSCOM 2012), Hong Kong
7. "Building Climate Change Resilience for Electricity Infrastructure," Power Grid Corporation of India, New Delhi, India (2015)
8. Press TNA (2017) Enhancing the resilience of the Nation's Electricity System. National Academies of Sciences, Engineering, and Medicine, Washington, DC
9. Ma J, Xu D, Wang T (2012) A novel method for multi-fault location utilizing fault fitting degree. In: 2012 IEEE Power and Energy Society General Meeting, San Diego, CA, USA.
10. González J (2013) Multiple fault diagnosis in electrical power systems with dynamic load changes using soft computing. Lecture Notes in Computer Science, Springer, Cham, vol. 7630.
11. Ashok V, Yadav A, Naik V (2018) Fault detection and classification of multi-location and evolving faults in double-circuit transmission line using ANN. In: Soft computing in data analytics. Springer, Singapore, pp 307–317
12. Swetapadma A, Yadav A (2015) Improved fault location algorithm for multilocation faults, transforming faults and shunt faults in thyristor controlled series capacitor compensated transmission line. IET Gener Transm Distrib 9(13):1597–1607
13. Na S, Kishor N, Uhlen K, Mohanty S (2013) Detecting instant of multiple faults on the transmission line and its types using time–frequency analysis. IET Gener Transm Distrib 13(22):5248–5256
14. Abdullah A, Butler_Purry K (2018) Distance protection zone 3 mal operation during system wide cascading events: The problem and a survey of solutions. Electric Power Syst Res 154:151–159
15. Shalini S, Samantaray, Sharma A (2018) Supervising zone-3 operation of the distance relay using synchronised phasor measurements. IET Generation Transmisssion Distribution 13(8).
16. Aghamohammadi M, Hashemi S, Hasanzadeh A (2016) A new approach for mitigating blackout risk by blocking minimum critical distance relays. Int J Electric Power Energy Syst 75:162–172
17. Abidin A, Mohamed A, Shareef H (2013) Power swing and voltage collapse identification schemes for correct distance relay operation in power system. J Central South Univ 20:988–1000
18. Mallikarjuna B, Reddy-Maddikara J (2019) Synchrophasor measurement-assisted system integrity protection scheme for smart power grid. J Control Automation Electrical Syst 31:207–225
19. Shalini, Samanatray S, Sharma A (2019) Enhancing performance of wide-area back-up protection scheme using PMU assisted dynamic state estimator. IEEE Trans Smart Grid 10:5066–5074.
20. Raoufi H, Vahidinasab V, Mehran K (2020) Power systems resilience metrics: a comprehensive review of challanges and outlook. Sustainability MDPI 12(22).
21. Kwasinski A (2016) Quantitative model and metrics of electrical grids' resilience evaluated at a power distribution level. Energies 9(2):93
22. Chanda S, Srivastava AAK (2016) Defining and enabling resiliency of electric distribution systems with multiple microgrids. IEEE Trans Smart Grid 7(6):2859–2868
23. Bajpai P, Chanda S, Srivastava A (2016) A novel metric to quantify and enable resilient distribution system using graph theory and choquet integral. IEEE Trans Smart Grid 9(4):2918–2929
24. Liu X, Shahidehpour M, Li Z et al. (2016) Microgrids for enhancing the power grid resilience in extreme conditions. IEEE Trans. Smart Grid 8(2):589–597.
25. Fisher R, Bassett G, Buehring W, Collins M, Dickinson D, Eaton L, Haffenden R, Hussar N, Klett M (2010) Constructing a resilience index for the enhanced critical infrastructure protection program. Argonne National Laboratory, Chicago, IL, USA.
26. Fisher R, Bassett G, Buehring W, Collins M, Dickinson D, Eaton L, Haffenden R, Hussar N, Klett M (2013) Resilience measurement index: an indicator of critical infrastructure resilience. Argonne National Laboratory, Chicago, IL, USA.
27. Panteli M, Mancarella P, Trakas D, Kyriakides E, Hatziargyriou N (2017) Metrics and quantification of operational and infrastructure resilience in power systems. IEEE Trans Power Syst 32:4732–4742
28. Panteli M, Mancarella PP (2015) The grid: Stronger, bigger, smarter? Presenting a conceptual framework of power system resilience. IEEE Power Energy Mag 13:58–66
29. Lei S, Wang J, Chen C, Hou Y (2018) Mobile emergency generator pre-positioning and real-time allocation for resilient response to natural disasters. IEEE Trans Smart Grid 9:2030–2041.
30. Panteli M, Pickering C, Wilkinson S, Dawson R, Mancarella P (2017) Power system resilience to extreme weather: Fragility modeling, probabilistic impact assessment, and adaptation measures. IEEE Trans Power Syst 32:3747–3757
31. Espinoza S, Panteli M, Mancarella P, Rudnick H (2016) Multi-phase assessment and adaptation of power systems resilience to natural hazards. Electr Power Syst Res 2016:352–361
32. Kasztenny B, Finney D (2008) Fundamentals of distance protection. In: 61st Annual Conference for Protective Relay Engineers. TX, USA
33. "Line Protective Relay User Manual Version 3.3," ERL Phase Power Technologies (2003).
34. Phadke A, Thorp J (2008) Synchronized phasor measurements and their applications. Springer, Cham.
35. Bie Z, Lin G, Li F (2017) Battling the extreme: a study on the power system resilience. Proc IEEE 105(7):1253–1266
36. Zhang H, Yuan H, Li G, Lin Y (2018) Quantitative resilience assessment under a tri-stage framework for power systems. Energies 11(6):1427
37. Rajalwal N, Ghosh D (2020) Superseding mal-operation of distance relay Under stressed systems conditions. In: Wide area power systems stability, protection, and security. Springer, Cham, pp 393–421.